Super-Resolution Imaging Through Stochastic Switching and Localization of Single Molecules: An Overview

Ke Xu, Sang-Hee Shim, and Xiaowei Zhuang

Abstract The resolution of fluorescence microscopy had traditionally been limited to ~200–300 nm due to the diffraction of light. Recently, this resolution limit has been broken using mainly two classes of methods, one of which utilizes photoswitching of fluorophores to temporally separate the spatially overlapping images of individual molecules such that the positions of these molecules can be precisely determined. A sub-diffraction-limit image can then be reconstructed from these molecular coordinates. With relatively simple optical instrumentation and sample preparation, this class of methods has improved the spatial resolution of far-field optical microscopy by more than an order of magnitude, achieving resolutions down to sub-10 nm range for biological specimens. Three-dimensional, multicolor, and live-cell super-resolution imaging has been demonstrated. In this chapter, we provide an overview of this class of optical nanoscopy, primarily in terms of the imaging principle, the spatial/temporal resolution, the different imaging schemes, the photoswitchable probes, the applications, and future directions.

Keywords (F)PALM · diffraction limit · photoswitching · single molecule · STORM · super-resolution microscopy

---

Authors Ke Xu and Sang-Hee Shim contributed equally to this chapter

K. Xu and S.-H. Shim
Department of Chemistry and Chemical Biology, Harvard University, Cambridge, MA 02138, USA

X. Zhuang (✉)
Department of Chemistry and Chemical Biology, Howard Hughes Medical Institute, Harvard University, Cambridge, MA 02138, USA

Department of Physics, Harvard University, Cambridge, MA 02138, USA
e-mail: zhuang@chemistry.harvard.edu

P. Tinnefeld et al. (eds.), *Far-Field Optical Nanoscopy*,
Springer Ser Fluoresc (2015) 14: 27–64, DOI 10.1007/4243_2013_61,

Contents

1 Background

1.1 Optical Microscopy and the Diffraction Limit

Optical microscopy is a widely used and indispensable imaging modality in biological studies. When compared to other microscopy techniques, optical microscopy, in particular fluorescence microscopy, provides the distinct advantages of being relatively noninvasive and molecularly specific. The former advantage permits the observation of live cells, tissues, and organisms. The latter, accomplished through fluorescent labels, allows for the specific observation of molecular targets with high contrast.

However, conventional optical microscopy has a resolution limit, typically on the order of several hundred nanometers, below which the structural details of the specimen can no longer be resolved. This limit is due to the wave-like nature of light. The far-field optical image of even an idealized point object will be blurred into a finite-sized spot due to diffraction, and the size of the spot is comparable to the wavelength of the light. The intensity distribution of this spot is called the point spread function (PSF). Under optimal imaging conditions with a high numerical aperture objective, the full width at half maximum (FWHM) of PSF for visible light is 200–300 nm in the lateral dimensions and 500–800 nm in the axial dimension. Hence, objects separated by a distance smaller than the width of the PSF will have overlapping images that cannot be resolved − in other words, the width of the PSF defines the resolution limit of conventional optical microscopy.

In recent years, several methods have been developed to break this conventional resolution limit imposed by diffraction. These methods are collectively called super-resolution fluorescence microscopy. One class of methods overcomes the diffraction limit by effectively reducing the size of the PSF using specially engineered illumination patterns. Examples in this category include stimulated emission depletion (STED) microscopy, microscopy taking advantage of reversible saturable optically linear fluorescence transitions (RESOLFT), and [saturated/non-linear] structured-illumination microscopy ([S/NL]SIM), which are covered in other chapters of this book.

In this chapter, we will focus on a different approach to super-resolution imaging, which resolves overlapping PSFs by the stochastic switching and localization of individual fluorophores.

1.2 Single, Isolated Fluorophores Can Be Localized with Nanometer Precision

Although diffraction inevitably results in a PSF several hundred nanometers in size for a point source of light, the position of the point source can nonetheless be localized with nanometer precision by determining the centroid of the PSF. The shape of the PSF can be determined either theoretically or experimentally. Therefore, the centroid positions of the PSFs can be readily obtained by fitting to known functions.

The theoretical PSF of a single point source of light is an Airy disk, but a simple two-dimensional (2D) Gaussian function provides a good approximation for ease of fitting [1, 2]. The fitting can be done with a precision that depends on the number of photons collected [2]. Experimentally, localization precisions as high as ~1 nm were first demonstrated for individual beads [3]. With the advent of single-molecule imaging [4], similar localization precisions were also achieved for individual fluorescent molecules [5, 6].

However, the nanometer-scale precision achieved in the localization of individual molecules does not directly translate into a high imaging resolution for densely labeled samples. This is because when the separation between adjacent fluorescent molecules is smaller than the diffraction limit, the PSFs of these molecules will overlap substantially, preventing the precise localization of the individual molecules. Early strategies to circumvent this problem include separation by orthogonal properties [7], such as color [8–10], sequential photobleaching of individual fluorophores [11, 12], and the blinking of individual quantum dots [13, 14]. These methods were able to resolve a few fluorophores per diffraction-limited area. On the other hand, for general super-resolution imaging with resolution substantially beyond the diffraction limit, many more fluorophores (hundreds to thousands) have to be resolved within a diffraction-limited area (see also Sect. 3.2), and new strategies are required.

2 Super-Resolution Imaging Through Stochastic Switching and Localization of Single Molecules

Recently, it was realized that the otherwise overlapping PSFs from densely labeled fluorophores can be separated in the time domain by employing fluorophores that can be switched between a non-emitting (dark) state and an emitting (fluorescent) state [15–17]. In this approach, at any given instant during imaging, the majority of the labeled fluorophores in the sample are maintained in the dark state, and only a small, random subset of the fluorophores are switched to the fluorescent state, typically using a weak activation laser (Fig. 1a). The number of simultaneously emitting fluorophores is kept sufficiently low that the PSFs of individual emitting fluorophores are isolated from each other; the location of each fluorophore can then be determined with nanometer precision using centroid fitting. The emitting fluorophores are then either optically switched back into the dark state or photobleached. Subsequently, another small, random subset of the labeled fluorophores is activated into the fluorescent state, and the locations of the newly activated molecules are again recorded. Iterating this procedure over time will eventually allow the locations of all (or a sufficiently large number of) the labeled fluorophores to be mapped, from which a super-resolution image can be constructed (Fig. 1).

This general strategy of super-resolution microscopy by stochastic switching and localization of single molecules has been originally introduced as stochastic optical reconstruction microscopy (STORM) [15], photoactivated localization microscopy (PALM) [16], and fluorescence photoactivation localization microscopy (FPALM) [17]. Both photoswitchable fluorescent dyes and photoactivatable fluorescent proteins can be used for sub-diffraction-limit imaging using this strategy.

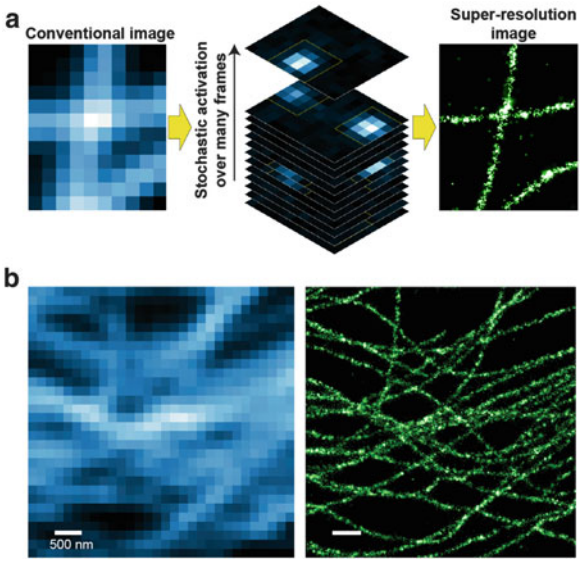

Fig. 1 The basic principles of STORM/(F)PALM. (**a**) Schematics illustrating the imaging concept. During the imaging process, only a small, optically resolvable subset of fluorophores are activated into the fluorescent state and subsequently localized with high precision at any given instant. The localized fluorophores are then switched back into the dark state and a new subset is activated. The cycle of switching and localizing repeats until a sufficient number of points are accumulated to reconstruct a super-resolution image. (**b**) Comparison of the conventional fluorescence image (*left*) of microtubules immunolabeled with Alexa 647 in a BS-C-1 cell with the STORM image (*right*) of the same area [18]. Scale bars: 500 nm. Figure adapted from reference [19]

More recently, the range of fluorescent probes that can be used for STORM/(F)PALM imaging has been substantially expanded through the realization that many conventional fluorescent dyes can in fact be photoswitched between fluorescent and dark states (a phenomenon also known as "blinking"), as demonstrated in PALMIRA (PALM with independently running acquisition) [20, 21], GSDIM (ground state depletion followed by single molecule return) [22], dSTORM (direct STORM) [23], single-molecule blinking microscopy [24], and fluorescence localization nanoscopy [25], etc. Along the same line, it is worth noting that a commonly used fluorescent protein, EYFP, can also be photoswitched between a fluorescent state and a dark state [26] and used for super-resolution imaging [27].

Photoswitching is not the only way to temperately separate overlapping images of single molecules to accomplish sub-diffraction-limit resolution. An elegant method called PAINT (points accumulation for imaging in nanoscale topography) [28] uses reversible binding of fluorescent molecules to target structures to accumulate numerous localizations and reconstruct super-resolution images. More recently, reversible binding of fluorescence quenchers has also been used to achieve the same goal [29].

Finally, due to the recent development on image analysis, the condition of well-isolated images of single molecules does not need to be rigorously satisfied for high-precision localization of individual molecules. Fluorophores with partially overlapping images can be localized using simultaneous multi-emitter fitting [30–32] and global optimization using compressed sensing [33]. Super-resolution imaging can also be accomplished by taking conventional movies and subtracting subsequent frames to reveal the transient blinking or bleaching of isolated single fluorophores using approaches called BALM (bleaching/blinking assisted localization microscopy) [34] and gSHRIMP (generalized single molecule high-resolution imaging with photobleaching) [35]). A Bayesian analysis of blinking and bleaching fluorophores (3B) [36] has been developed to model the entire fluorescence movie with an ensemble of most likely fluorophore locations. Super-resolution images can even be derived without localizing individual molecules but through correlation analysis (super-resolution optical fluctuation imaging (SOFI) [37] or nonlinear image deconvolution (decon-STORM) [38] of movie frames comprised of partially overlapping emitters. Many of these methods increase the number of molecules that can be imaged per camera frame and thereby substantially improve the imaging speed.

3 Image Resolution

3.1 Localization Precision and the Optical Resolution

The optical resolution of these molecular-localization-based super-resolution methods is ultimately determined by the precision with which each fluorophore can be localized. The theoretical limits of the localization precision are well established [2]. For a single point source, each detected photon can be viewed as an independent report of its location. As each photon is randomly distributed according to the PSF (with width Δ), a localization precision of $\sim \Delta/N^{1/2}$ can be expected when N photons are collected from the same point source. More sophisticated models also include the effects of background noise and the pixel size of the camera [2].

Experimentally, the localization precision can be determined by repeatedly measuring the position of a single fluorophore and determining the standard deviation (SD) of the localization distribution. For example, localization precisions of ~8 nm (SD) per switching cycle have been demonstrated for bright, photoswitchable dyes Cy5 and Alexa 647 [15, 18, 39]. Approximately 2x worse localization precision has been achieved with some of the dimmer dyes (e.g., Atto 488 and DyLight 750) and fluorescent proteins (e.g., tdEos and mEos2) [40, 41].

In the literature, both standard deviation (SD) and full width at half maximum (FWHM) have been used to characterize the optical resolution for localization-based super-resolution imaging methods, which potentially creates confusion in the comparison of different measurements. For Gaussian distributions, FWHM $= 2.35$ SD. FWHM is a better representation of the imaging resolution as it corresponds to

the smallest separation between two probes that can be resolved. In this chapter, we will use the FWHM value when discussing resolution.

It is also worth noting that the experimentally determined localization precision values are substantially worse (typically by twofold) than the theoretically predicted values. This indicates that the theoretical values do not faithfully represent the actual localization precision. Factors limiting the actual localization precision include camera noise, background noise, nonuniformity of the camera pixels [6], mechanical instability of the instrument, errors in data analysis, and any other imperfections of the imaging and analysis systems.

Besides the localization precision of single fluorophores, the resolvability for actual biological structures is also affected by how faithfully the labels represent the structures of interest. Any sizable label, such as antibodies (~10 nm in size) and fluorescent proteins (~4 nm in size), will substantially affect the image resolution when the resolution becomes comparable to the label size.

3.2 Localization Density and the Nyquist Resolution Limit

Super-resolution methods provide an optical resolution that sometimes approaches the distance between adjacent labels in a sample. At this level, not only does the localization precision of each label but also the label density and efficiency affect the final image resolution.

For continuous structures, the effects of labeling density can be quantified using the Nyquist-Shannon sampling criterion, which states that structural details smaller than twice that of the average label-to-label distance cannot be reliably resolved [42]. Formally, this Nyquist resolution limit can be expressed as $2/N^{1/D}$, where N is the number density of labels and D is the dimensionality of the image. To achieve Nyquist resolutions that are comparable to the optical resolution (i.e., the localization precision) of ~20 nm, a labeling density of $\sim 10^4/\mu m^2$ is required for 2D imaging. It should be noted, however, that due to the spatial inhomogeneity of biological structures, the same Nyquist resolution can often be achieved at lower *overall* localization densities, as long as the *local* localization density of the structure of interest is sufficiently high. The final image quality is affected by both the optical resolution based on localization precision and the Nyquist resolution limit determined by the label or localization density: Whichever is worse (larger in value) dominates the effective image resolution. When the two resolutions are comparable, the convolution of the two may be employed to represent the final resolution [41]. It is also worth noting that the localization density is not only limited by the label density but also by the on-off duty cycle of the photoswitchable probes, namely, the fraction of time each probe spends in the on state [40]. Because multiple probes emitting at the same time within a diffraction-limited area generate overlapping images that reduce the localization precision, fluorophores with a duty cycle of 1/N typically allow less than N molecules to be localized within a diffraction-limited area.

For super-resolution studies on the distributions of sparsely distributed molecules, the Nyquist resolution is less relevant, because the molecular structure itself does not allow a high labeling density. Nonetheless, high labeling efficiency (fraction of molecules being labeled) is still required for faithfully mapping out the underlying distribution.

4 Three-Dimensional Imaging

Most biological samples are three-dimensional (3D), and thus defining their structural details requires 3D super-resolution imaging. STORM, (F)PALM, and related methods achieve super-resolution through the localization of individual molecules; hence, to acquire 3D imaging capability entails the determination of the 3D locations of single emitting molecules. While the lateral position (x- and y-coordinates) of a fluorophore can be readily determined from the centroid of the PSF, the determination of the axial position (z-coordinate) requires additional manipulation and analysis of the PSF. Nonetheless, it can be done with a variety of methods, many of which were first developed in earlier studies for single-particle tracking and spectrally selective imaging, including fitting the shape of the PSF [43–49], interferometry [50, 51], and tilted mirrors [52].

4.1 PSF Shape-Based Methods: Astigmatism and Multifocal Plane Detection

An obvious difference between the PSFs of fluorophores with different axial positions is their apparent width. When projected onto the image plane (the camera), fluorophores right at the focal plane of the microscope produce the smallest images, whereas defocused fluorophores produce larger PSF. One could thus derive the z-information of individual molecules from the measured PSF width. The problem with directly applying this defocusing approach is that molecules above and below the focal plane have similarly broadened PSF.

To break this symmetry, 3D super-resolution imaging was first realized by the introduction of astigmatism into the imaging system [39]. Specifically, a cylindrical lens is introduced into the imaging path (Fig. 2a). As a result, the images of individual molecules become elliptical, and elongated in two orthogonal directions for molecules above and below the focal plane (Fig. 2a). The axial position of each molecule can thus be obtained from the ellipticity of the observed PSF, which in combination with the lateral positions obtained from the centroids of the PSF, leads to the 3D reconstruction of super-resolution images (Fig. 2b). The astigmatism method provides a resolution ~25 nm in xy and ~50 nm in z when imaging a bright photoswitchable fluorophore Cy5 (or its structural analog Alexa 647). Here, we

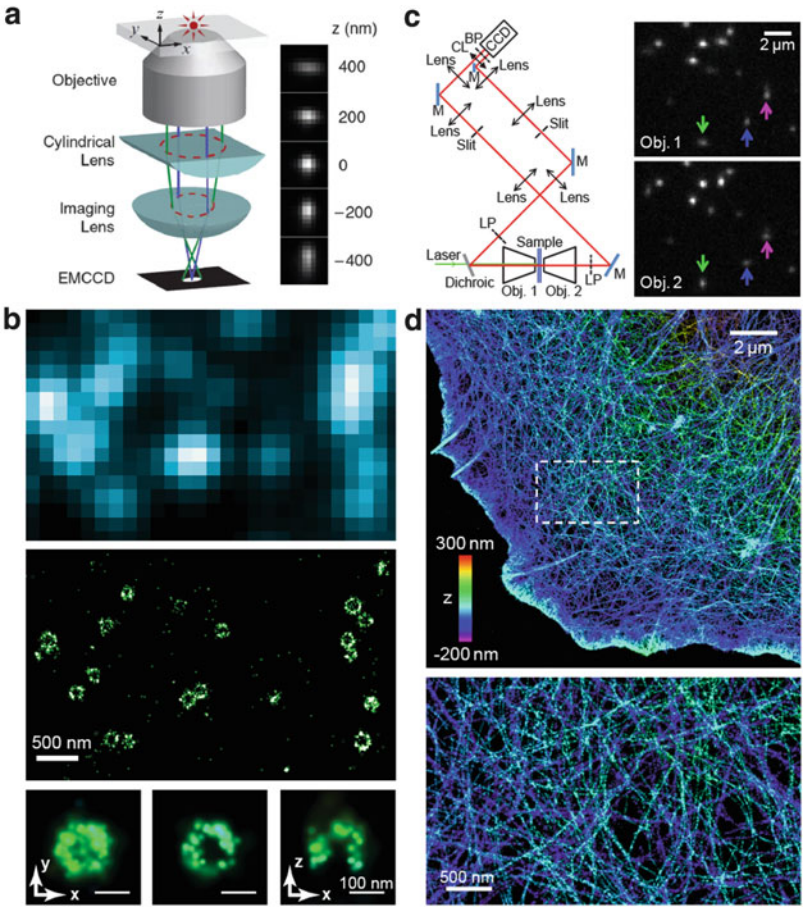

Fig. 2 Astigmatism-based three-dimensional STORM imaging. (**a**, **b**) 3D STORM imaging using a single objective. Figure adapted from reference [39]. (**a**) Schematics of the setup (*left*) and the experimentally observed images of a single fluorophore as its *z*-position was varied (*right*). A cylindrical lens is used to introduce astigmatism into the imaging system, such that elliptical images with long axes along two orthogonal directions are observed for fluorophores above and below the average focal plane. The *z*-position of each fluorophore can thus be obtained from the ellipticity of the observed image. (**b**) Conventional image (*top*) of immunolabeled clathrin-coated pits in a mammalian cell, in comparison with the corresponding 3D STORM image (*middle*) showing an *xy* cross section near the plasma membrane. *Bottom panel*: Magnified STORM images of a single clathrin-coated pit with an *xy* projection (*left*), an *xy* cross section near the plasma membrane (*center*), and an *xz* cross section cutting through the middle of the pit (*right*) (**c**, **d**) Dual-objective 3D STORM further improves image quality. Figure adapted from reference [53]. (**c**) *Left panel*: Schematic of the dual-objective setup. Two microscope objectives are placed facing each other and focused on the same spot of the sample. Astigmatism is introduced into the images collected by both objectives using a cylindrical lens. *M* mirror, *Obj.* objective, *LP* long-pass filter, *CL* cylindrical lens, *BP* band-pass filter. *Right panel*: Images of single molecules obtained from two objectives in a single frame. A molecule that appears elongated in *x* through one objective should appear elongated in *y* through the opposing objective, and vice versa

again use the FWHM values for 3D resolution as we did for 2D resolution because it is a better representation of the closest resolvable separation between objects. Using the astigmatism-based approach, a range of ~600–800 nm in z can be imaged without scanning [39]. This method remains the simplest approach to 3D super-resolution imaging.

The resolution of astigmatism-based 3D imaging can be further improved by the introduction of a second objective lens facing the first objective (Fig. 2c, d) [53]. This modification doubles the number of collected photons, provides a noise-canceling mechanism due to the anticorrelated ellipticity detected from the two objectives (Fig. 2c), and improves the mechanical stability of the setup. The combination of these effects led to a substantially improved resolution of 10 nm in xy and 20 nm in z when imaging Alexa 647 [53].

In a different defocusing approach, biplane imaging was carried out to achieve sub-diffraction-limit resolution in three dimensions by splitting the emitted fluorescence into two optical paths with different path lengths [54]. The z-positions of individual fluorophores were obtained by comparing the defocused PSF shapes at the two different image planes with the expected 3D PSF. An axial resolution of 75 nm was demonstrated when using caged fluorescein as the probe, with a ~800 nm z-imaging range without moving the sample [54].

While the use of PSF shape alone to determine the z-position can be more readily implemented with conventional optics, the z-resolution of these methods is limited to ~2x the lateral resolution due to the fact that the 3D PSF itself is wider in the axial direction than in the lateral directions. To achieve higher resolution in z, the phase information of the emitted photons can be used. Although the phase information provides a means to achieve higher z-resolution, the experimental implementation is often more complicated (Fig. 3a, c) and poses difficulties for emission-based multicolor imaging (see Sect. 5.2). We describe these phase-based approaches below.

4.2 PSF Engineering Through Fourier Optics

Phase information can be encoded into the PSF shape by the use of a predesigned phase mask (typically created using a spatial light modulator) placed at the Fourier plane of a 4-*f* imaging system (Fig. 3a). It has been shown that the PSF of individual fluorophores can be engineered to have two lobes that rotate as a function of the axial

Fig. 2 (continued) (e.g., *green* and *blue arrows*). In contrast, if two nearby molecules were mistaken for a single molecule, the images obtained through both objectives would appear elongated in the same direction along the line that connects the two molecules (e.g., *magenta arrows*). (**d**) Dual-objective 3D STORM resolves individual actin filaments in cells. *Top panel*: Dual-objective STORM image of actin (labeled with Alexa 647-phalloidin) in a COS-7 cell. *Bottom panel*: Close-up of the boxed region in the *top panel*. z-positions are color coded according to the color bar in the *top panel*

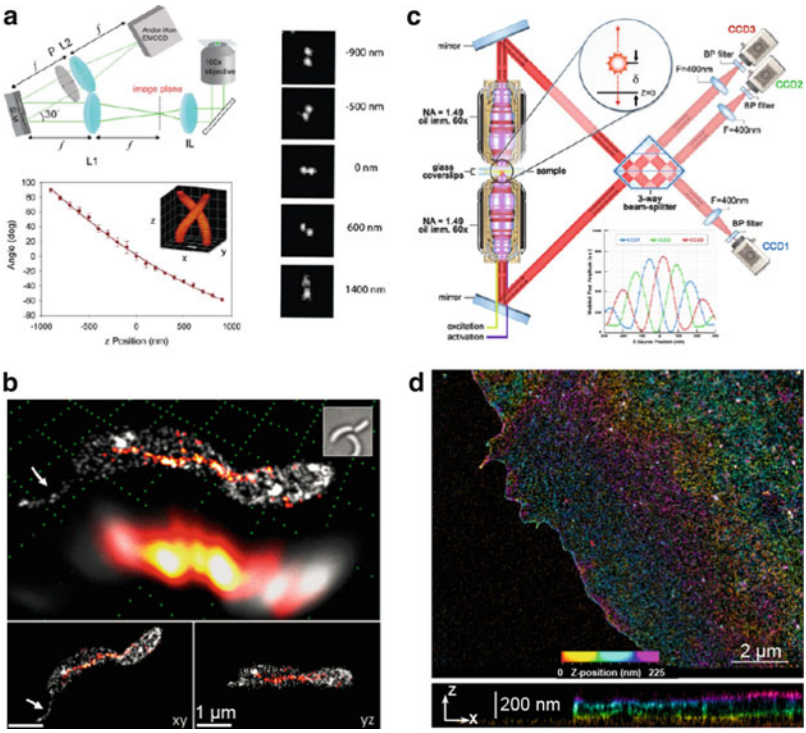

Fig. 3 Three-dimensional super-resolution imaging using double-helix PSF and single-molecule interferometry. (**a**, **b**) Double-helix PSF-based 3D imaging. (**a**) Schematics of the setup and *z*-calibration. Figure adapted from reference [55]. A spatial light modulator (SLM) loaded with a predesigned phase mask is placed at the Fourier plane of a 4-*f* imaging system, leading to two-lobe-shaped PSFs for individual fluorophores. The two lobes rotate as a function of the axial position of the fluorophore, thus providing *z*-information for each fluorophore. (**b**) Double-helix PSF 3D super-resolution imaging of CreS-eYFP (*red-orange*) and cell membrane (*gray*) in *Caulobacter crescentus*. *Top panel*: Super-resolution and diffraction-limited perspective images. *Bottom panel*: Two-dimensional isometric *xy* and *yz* projections. Figure adapted from reference [60]. (**c**, **d**) An example of the interferometry-based approach. Figure adapted from reference [57]. (**c**) Schematic of the setup. The fluorescence of individual fluorophores is collected by two objectives from opposing sides of the sample. The fluorescence photons interfere with themselves at the beam splitter, generating intensity interference patterns that are determined by the *z*-position of the fluorophore (*inset*). (**d**) Interferometry-based 3D super-resolution image of a COS-7 cell expressing the membrane protein VSVG that is fused to the photoconvertible FP, tdEos. *Bottom panel*: The *x*-*z* cross section of the boxed region in the *top panel*

position of the fluorophore (Fig. 3a) [55]. The resultant double-helix PSF (DH-PSF) therefore provides the *z*-information of each fluorophore by the orientation of the two lobes, allowing for 3D super-resolution imaging (Fig. 3b). A *z*-resolution of ~50 nm (FWHM) was demonstrated for the DCDHF dye. More recently, a PSF with a single-helix (SH-PSF) shape has also been created for 3D super-resolution imaging [56].

Compared to the defocusing approaches described above, an advantage of these helical PSF approaches is the longer z-range (~2 μm) that can be imaged without scanning the focal plane (Fig. 3a, b) [55]. A potential disadvantage of these approaches is that the PSF in these cases takes up a larger imaging area, which could limit the number of fluorophores that can be simultaneously imaged in each frame and thus lead to slower data acquisition. The use of a polarization-dependent spatial light modulator can also lead to a reduction in the number of photons collected at the camera.

4.3 Single-Molecule Interferometry

Interferometry-based single-molecule localization provides a direct way to extract phase information [57–59]. A single photon is coherent with itself; therefore, self-interference of individual photons will lead to intensity modulation of the signal from a single fluorophore. In this approach, photons emitted from individual fluorophores are collected by two objectives from opposing sides of the sample and self-interfered at a beam splitter, generating intensity modulations due to path-length differences determined by the axial position of the fluorophore (Fig. 3c). Using this approach, z-resolutions as high as ~10 nm have been demonstrated when using fluorescent proteins (Fig. 3d) [57] and organic dyes [59].

A major drawback of the interferometry-based method is the complexity in instrumentation, partly due to the short coherence length of fluorophores (a few micrometers). In its first implementation, the interferometry-based method was limited to samples thinner than ~200 nm because the interference pattern repeats itself every one-half of the emission wavelength [57]. In a subsequent work, this limitation was overcome by considering the spherical shape of the wavefront and examining the higher moments of the PSF, extending the working z-range to ~600 nm [59].

4.4 Tilted Mirrors

By projecting the axial dimension onto a lateral dimension using a tilted mirror, virtual volume super-resolution microscopy (VVSRM) determines the 3D position of single fluorescent emitters through observing the side-view mirror reflection (virtual image) alongside with the front-view real image [61]. VVSRM is capable of providing near-isotropic 3D resolution, but the requirement of sample being positioned close to (or attached to) a specialized, tilted micro-mirror potentially limits broader application of the method.

4.5 Thick Sample Imaging

Due to the relatively small depth of focus for high NA objectives (~600 nm, which essentially *defines* the axial resolution of conventional optical microscopy), most 3D localization techniques have a similar, limited working z-range of ~600–800 nm (except for the helical PSF methods). A natural way to extend the z-range is to scan the focal plane in steps smaller than ~600 nm and stack up the 3D super-resolution images acquired at each step [54, 62]. For example, by combining astigmatism-based imaging and z-scanning, whole-cell 3D super-resolution images were demonstrated with z-ranges of ~3 μm [62]

Although relatively easy to implement, a drawback to the direct application of z-scanning is that during imaging, illumination is not restricted to the volume being imaged. This leads to undesired activation and excitation of fluorophores outside the focal volume, causing increased fluorescence background and unnecessary photobleaching.

The illumination problem can be alleviated by the use of two-photon absorption, which, through nonlinear optical processes, is capable of confining the activation of fluorophores to a thin layer near the focal plane. This technique was first combined with 2D super-resolution imaging to generate 3D image stacks that only achieve super-resolution in the lateral directions [63, 64]. More recently, optical sectioning with two-photon activation was combined with astigmatism-based 3D super-resolution imaging, allowing a total imaging depth of up to ~7 μm [65].

Another way to confine the illumination axially is to use thin light sheets. In selective plane illumination microscopy (SPIM), the excitation light is shaped into a thin sheet that illuminates the sample through a separate objective placed perpendicular to the detection objective. Sheet illumination allows optical sectioning and prevents photobleaching and photoactivation outside the focal region [66]. Individual molecule localization-SPIM (IML-SPIM) was demonstrated by shaping the activation and excitation beams into collinear light sheets [67]. In combination with astigmatism for 3D localization, IML-SPIM achieved 63-nm lateral resolution and 140-nm axial resolution for thick specimens at a depth of 50–100 μm.

5 Multicolor Imaging

Multicolor imaging is one of the key advantages of fluorescence microscopy. With proper labeling, multicolor imaging allows for the visualization of different target molecules in a sample, from which the spatial relations and interactions between different molecules can be inferred. Multicolor super-resolution imaging has been accomplished using STORM, (F)PALM, and related methods by using fluorescent probes with different wavelengths of activation or emission.

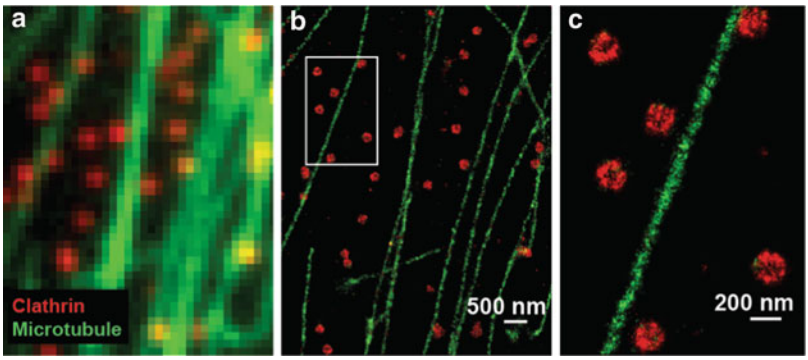

Fig. 4 Multicolor super-resolution imaging: activation-based approach. Antibodies labeled with Cy2 and Alexa 647 (*green*) and antibodies labeled with Cy3 and Alexa 647 (*red*) were used to stain the microtubules (*green*) and clathrin (*red*) in a BS-C-1 cell, respectively. Two-color imaging was achieved by alternating between two activation lasers (457 and 532 nm) and an excitation laser (657 nm). Figure adapted from reference [18]. (**a**) Conventional fluorescence image. (**b**) Corresponding STORM image. (**c**) Close-up of the boxed region in *b*

5.1 Activation-Based Multicolor Imaging

While photoswitchable dyes are typically activated to fluorescent states by illumination with ultraviolet (UV) light, the activation wavelength can be shifted into the visible range for some photoswitchable dyes by pairing them with another dye molecule that absorbs visible light. Upon absorbing light, the latter dye molecule (called an activator) can facilitate the activation of the photoswitchable dye (called a reporter). For example, by pairing the same reporter dye, Cy5, with three different activator dyes, Alexa Fluor 405, Cy2, and Cy3, the Cy5 dye can be activated into the fluorescent state when illuminated by violet, blue, or green light, respectively [18]. Multicolor imaging can thus be performed using these photoswitchable dye pairs, in which case the same reporter dye is imaged and localized in all color channels, but the different dye pairs are distinguished by the different wavelengths of light used for activation (Fig. 4) [18]. As a result, the images in different color channels are always perfectly aligned since the same optical path was used to collect the fluorescence emitted by the reporter in different dye pairs. In addition, the activation-based multicolor approach allows one to pick the best reporter dye to achieve the highest image resolution in all different color channels.

It should be noted that the light used to image the reporter dye can also directly activate the dye, albeit with a low activation rate. On the plus side, this property allows a very simple-imaging scheme for single-color super-resolution imaging with a single-color laser source and single photoswitchable reporter [68]. On the flip side, for multicolor imaging, this property leads to a drawback of relatively high color crosstalk. During imaging, activation by the imaging light results in nonspecific localizations independent of the activation light. This effect can lead to substantial

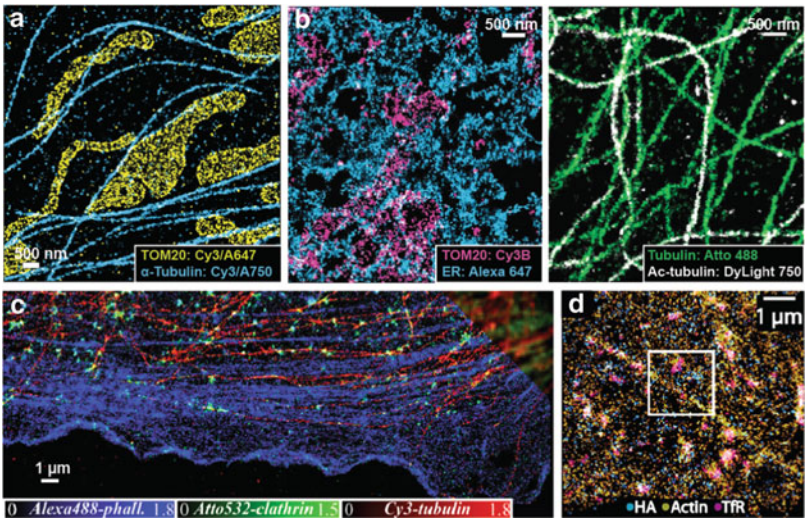

Fig. 5 Multicolor super-resolution imaging: emission-based approaches. (**a**, **b**) Examples in which emitters with well-separated emission spectra were used. (**a**) Dual-emission channel super-resolution imaging of microtubules (*cyan*) and mitochondria (*yellow*) in BS-C-1 cells immunostained with the Cy3-Alexa 750 dye pair and the Cy3-Alexa 647 dye pair, respectively. Figure adapted from reference [69]. (**b**) Four-color super-resolution image of a fixed BS-C-1 cell stained for the endoplasmic reticulum (ER), mitochondria, microtubules, and acetylated tubulin [40]. *Left panel*: Two of the four color channels, showing Alexa 647-labeled ER (*cyan*) and Cy3B-labeled mitochondria (*magenta*). *Right panel*: The other two color channels of the same image, showing Atto 488-labeled microtubules (*green*) and DyLight 750-labeled acetylated tubulin (*white*). Figure adapted from reference [40]. (**c**, **d**) Examples in which emitters with overlapping emission spectra were used and color identification was achieved through a ratiometric method. (**c**) Three-color super-resolution image of Alexa 488-phalloidin-labeled F-actin (*blue*), Atto 532-labeled clathrin (*green*), and Cy3-labeled tubulin (*red*) in a fixed PtK2 cell. Figure adapted from reference [77]. A conventional wide-field image of the upper right corner of the field of view is shown for comparison. (**d**) Three-color super-resolution image of Dendra2-hemagglutinin (*cyan*), PAmCherry1-β-actin (*yellow*), and PAmKate-transferrin receptor (*magenta*) expressed in a fixed HAb2 cell. Figure adapted from reference [74]

crosstalk (10–20 %) between different color channels [69]. Although crosstalk subtraction [70] can reduce the crosstalk to below 10 %, when imaging molecules with very different abundance, crosstalk from the high-abundance species could overwhelm the signal from the low-abundance species.

5.2 *Emission-Based Multicolor Imaging*

Multicolor imaging can also be achieved by employing photoswitchable probes (emitters) with different emission colors (Fig. 5). Emission-based multicolor super-resolution imaging has been achieved using different-colored fluorescent

proteins [71–74], different-colored organic dyes [40, 41, 75–77], or a combination of fluorescent proteins and dyes [21]. A recent comprehensive dye screen led to the identification of high-quality photoswitchable dyes in four separate spectral regions and thus four-color super-resolution imaging (Fig. 5b) [40]. Three-color super-resolution imaging has also been accomplished with fluorescent proteins (Fig. 5d) [74].

Compared to the activation-based approach, the emission-based approach provides substantially lower color crosstalk (as low as a few percent) when the probes used have well-separated emission spectra (Fig. 5a, b). In the event that the emission spectra of the different probes overlap considerably, they can still be separately identified using ratiometric methods (Fig. 5c, d), though the crosstalk in this case tends to be higher (5–20 %) [74, 75, 77].

A drawback of the emission-based multicolor approach is that multiple filter sets and/or optical paths have to be employed. Aligning the images obtained from different color channels with nanometer-scale accuracy is nontrivial, especially since chromatic aberrations (and other imperfections) are hard to eliminate completely in the imaging system. Alignment of different color channels is typically performed using fiducial markers such as fluorescent beads with a broad emission spectrum [41]. In addition, not all photoswtichable probes have the same brightness (number of photons detected per switching event). The brightest photoswitchable probes (i.e., Cy5, Alexa 647) all tend to have the same (far-red) emission wavelength [40]. As a result, one or more channels will have compromised image resolution using emission-based multicolor imaging as compared to activation-based multicolor imaging. The use of probes with different emission spectra also creates problems for interferometry-based 3D imaging, though it is possible to solve these problems with probes of overlapping spectra using a ratiometric method [59].

Finally, when activator-reporter dye pairs are used, combination of the activation-based and emission-based approaches allows imaging with a large number of colors. For example, when three reporter dyes and three activator dyes are combined, as many as nine distinct dye pairs can be constructed. Six- and seven-color super-resolution imaging has recently been demonstrated using this combinatorial approach [69, 78].

6 Live-Cell Imaging

Live-cell imaging capability is another key advantage of optical microscopy, which allows direct visualization of molecular processes in cells in real time. The substantially improved spatial resolution of optical nanoscopy opens a new window for capturing ultrastructural dynamics in vivo. A number of important factors should be considered for live-cell imaging, including labeling living cells with photoswitchable probes, the trade-off between spatial and temporal resolutions, motion blurring effect, and potential phototoxicity to live samples. We discuss these points below.

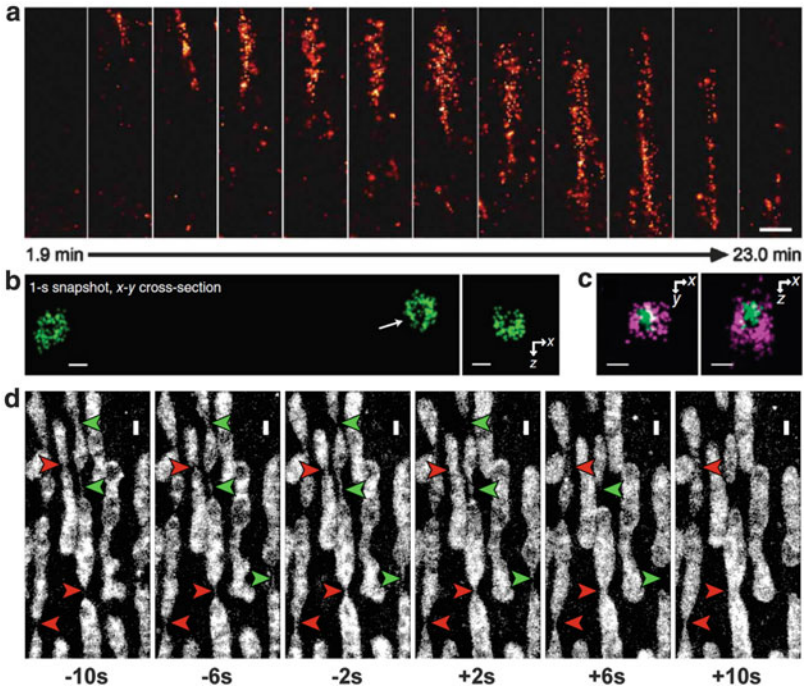

Fig. 6 Live-cell super-resolution imaging. (**a**) tdEos-tagged focal adhesion molecules imaged in 2D at 55-s time resolution in a live CHO cell. Figure adapted from reference [42]. (**b**) Alexa 647-SNAP-labeled clathrin-coated pits resolved in 3D at 1-s resolution in a live BS-C-1 cell. *Left panel*: An *x-y* cross section of clathrin-coated pits near the plasma membrane. *Right panel*: An *x-z* cross section through the middle of the coated pit indicated by the *arrow*. Figure adapted from reference [41]. (**c**) Two-color image of an Alexa 647-SNAP-labeled clathrin-coated pit (*magenta*) enclosing an Alexa 568-conjugated transferrin cluster (*green*) in a live BS-C-1 cell. *Left panel*: An *x-y* cross section near the plasma membrane. *Right panel*: An *x-z* cross section cutting through the middle of the pit. Figure adapted from reference [41]. (**d**) MitoTrackerRed-labeled mitochondria imaged at 2-s time resolution in a live BS-C-1 cell. Mitochondrial fusion (*red arrows*) and fission (*green arrows*) intermediates with tubular structures are observed with high resolution in real time. Figure adapted from reference [90]. Scale bars: (**a**) 5 μm, (**b**, **c**) 100 nm, (**d**) 500 nm

6.1 Labeling Live Cells with Photoswitchable Probes

The most straightforward method for labeling proteins in live cells with fluorescent probes is to use fluorescent proteins, which can be genetically fused to the target proteins of interest. Indeed, live-cell sub-diffraction-limit imaging using the stochastic switching was initially demonstrated with photoactivatable fluorescent proteins: PA-GFP, tdEos, or mEos2 in mammalian cells [42, 79] (Fig. 6a) and EYFP in bacteria [27]. To achieve relatively high resolution and avoid potential

artifacts due to the oligomerization tendency of fluorescent proteins, bright, monomeric proteins such as Dendra, mEos2, mEos3, PAmCherry, and PAtagRFP [73, 80–83] are preferred. On the other hand, these proteins can switch on only one to two times before photobleaching. For applications where many snapshots are required to follow the entire time course of a process, proteins with many switching cycles are required. The newly developed rsEGFP and Dreiklang, which can switch hundreds to thousands of cycles [84, 85], may be promising candidates.

Compared to fluorescent proteins, organic dyes tend to have superior brightness and faster switching rates, and thus offer higher spatial and temporal resolutions. Live-cell labeling of proteins with organic dyes, however, requires more steps than with fluorescent proteins: (1) the target protein needs to be genetically encoded with specific peptide or protein tags that can bind to or react with dyes; (2) dyes have to be delivered into live cells such that they can be attached to the specific tag. Live-cell super-resolution imaging has been demonstrated with various tags including SNAP, Halo, and trimethoprim [41, 77, 86–88]. For live-cell delivery, cell-permeable dyes are most convenient and these dyes, such as Atto 655, TMR, and OregonGreen, have been used for super-resolution imaging of living cells [77, 86, 88]. However, these dyes are not brighter (i.e., does not give more photons per switching cycle) than the above-mentioned fluorescent proteins and, hence, do not provide higher image resolution. The bright and fast switching dyes, such as Cy5 and Alexa 647, which yield ~4 times more photons than the cell-permeable dyes and fluorescent proteins in living cells, cannot spontaneously penetrate cell membrane. Nonetheless, they can be delivered into live cells by methods that temporally disrupt the cell membrane, such as electroporation, bead loading, and microinjection, providing substantially higher spatial and temporal resolution than affordable by fluorescent proteins [41] (Fig. 6b). One thing to note, however, is that switching characteristics of these cyanine dyes tend to be sensitive to their environment and the best performance often requires chemical additives such as thiols and oxygen scavengers; at low concentrations, these additives do not affect cell viability.

Small-molecule probes that directly bind to DNA or membrane can also be used for live-cell super-resolution imaging. These probes are often commercially available and easy to use. Also, the high labeling density, stemming from the small size and high affinity of these probes, improves the resolution and extends the length of time-lapse imaging. Nuclear and mitochondrial DNA were imaged in live cells with Picogreen [89]. Eight conventional membrane probes enabled live-cell imaging of the plasma membrane, mitochondria, ER, and lysosomes (Fig. 6d) [90].

Multicolor live-cell imaging has also been achieved using spectrally distinct fluorophores, either with fluorescent proteins [73] or fluorescent dyes (Fig. 6c) [41]. For fluorophores with partially overlapping spectra, ratiometric methods can be used for live-cell super-resolution imaging, again either using dyes, fluorescent proteins, or a combination between the two [74, 77, 90].

6.2 Spatial and Temporal Resolutions

In time-resolved super-resolution imaging, spatial and temporal resolutions intrinsically trade off with each other. For example, in the point scanning approaches, such as STED [91], the higher the resolution, the smaller the pixel size used on scanning and hence the slower the imaging speed. In the wide-field single-molecule-based approach, such as STORM and (F)PALM, the trade-off between spatial and temporal resolutions arises from the fact that a sufficiently large number of localizations need to be accumulated to resolve a structure at a desired Nyquist resolution (see Sect. 3.2 for definition of Nyquist resolution) [42]. Increasing the time window will result in more localizations, thereby improving the spatial resolution defined by the Nyquist criterion. Conversely, decreasing the time window for each STORM snapshot will improve the time resolution at the expense of the spatial resolution.

In live-cell studies using photoswitchable/photoactivatable fluorescent proteins, spatial resolutions of 40–70 nm have been achieved with 30–60 s time resolutions [27, 42] (Fig. 6a). Improving the time resolution may be difficult with the currently available fluorescent proteins as the number of photons detected per switching cycle tends to decrease when the excitation laser intensity was increased to accelerate the switching rate [41]. Hence, the camera frame rate used for imaging photoswitchable/photoactivatable fluorescent proteins is typically not higher than 100 Hz, beyond which the image quality deteriorates rapidly. This difficulty can be overcome with bright, fast switching fluorescent dyes, such as Alexa 647, which give a constant number of photons per switching cycle even when the off-switching rate is as fast as ~1 ms. Hence, STORM images using Alexa 647 could be recorded at the camera frame rate of 500–1,000 Hz, and cellular structures have been imaged in two dimensions with a Nyquist resolution of ~20 nm at time resolutions as high as 0.5 s [41].

For 3D imaging, substantially more localizations are required to define a structure with the same Nyquist resolution than in 2D given that the localizations are now spread across a 3D volume instead of a 2D projected area. For instance, a sphere with a 100-nm diameter would require only 80 localizations in 2D but 520 localizations in 3D to achieve a 20-nm Nyquist resolution. Hence, the temporal resolution of 3D super-resolution is typically lower than the 2D counterpart. Using Alexa 647 and astigmatism imaging, 3D super-resolution imaging has been achieved with a Nyquist resolution of 25–30 nm at 1–2-s temporal resolution (Fig. 6b) [41]. Another factor that reduces the 3D imaging speed is that the modified PSF for axial localization will cover a larger area, reducing the number of molecules that can be localized per frame, and hence the overall imaging speed. For example, the elliptically shaped PSF in astigmatism imaging [39], the isotropically expanded PSF in biplane imaging [54], and the rotating dumbbell PSF in DH-PSF imaging [55], all cover substantially larger area than the focused, circularly symmetric PSF used in 2D imaging. While the interferometry-based method [57] does not increase

the PSF size, the need to sandwich the sample between two objectives in this case considerably limits the applicability of such methods to live-cell imaging.

One way of improving the time resolution of live-cell imaging is to develop analysis methods that can fit multiple, partially overlapping PSFs simultaneously. Several analysis methods have been developed for these purposes, such as DAOSTORM [30, 32], multiple emitter fitting [31], 3B analysis [36], decon-STORM [38], and compressed sensing [33]. Such analysis methods allow for the activation of more molecules per frame, so the desired number of localizations can be collected in a smaller number of camera frames (and shorter time). SOFI [37], a super-resolution imaging method based on single-molecule fluctuation, also allows for fast live-cell super-resolution and will be described in detail in another chapter of this book.

6.3 Single-Molecule Tracking

The use of photoactivation also offers a unique opportunity to capture the dynamics of individual molecules in living cells. For example, single-particle tracking has been widely used to probe the motion (diffusion) of lipids and proteins on membranes in live cells [92]. However, to track individual molecules, the density of molecular images must be kept low enough that the images do not overlap. The low-density molecular traces make it difficult to provide both spatially and temporally resolved information about membrane diffusivity. Photoactivatable probes allow high-density single-molecule tracking in live cells by switching on an optically resolvable subset of photoactivatable probes at any time, tracking individual probes until photobleaching, and then repeating cycles of switching and tracking to accumulate a large number of trajectories [93]. Besides using photoactivation, binding/unbinding events can also be used to collect a high density of molecular trajectories on the cell surface as shown in PAINT [28, 94]. The time resolution of tracing individual molecules is limited by the camera frame rate, typically in the range of 30–1,000 Hz. The high-density map of molecular trajectories can be used to probe distinct subsets of molecules and can provide insight into spatial and temporal heterogeneities in the membrane [82, 93, 95], as well as in other systems.

6.4 Motion Blur

Unlike in fixed specimens, molecules and subcellular structures move in live cells. Their motion can effectively deteriorate spatial resolution and distort the observed structures. Two types of motions are important to consider for live-cell super-resolution imaging. The first type is the motion of probe molecules within

a camera frame (e.g., diffusion). A general rule of thumb is that, to maintain the localization precision, the probe molecule should not move by a distance larger than the localization error during a camera frame. For example, a molecule diffusing at 0.1 $\mu m^2\ s^{-1}$ on a membrane moves by 200 nm on average within 0.1 s and by 30 nm in 2 ms. Thus, a fast camera is essential for localizing fast-diffusing molecules with high precision. Additionally, the image shape of the molecule is blurred by diffusion within a camera frame, and therefore 3D imaging methods that rely on PSF shapes to obtain the axial position potentially require even faster frame rate. The plus side of molecular diffusion is that as the molecules diffuse within and map out the underlying structure, each probe molecule could contribute more than one independent localizations, which in turn improves the Nyquist resolution.

The second type of motion to consider is the motion/change of the structure itself during each super-resolution snapshot. To avoid artifacts due to this motion, the displacement/deformation of the structure during the time acquiring each snapshot should be less than the spatial resolution. Given that super-resolution methods provide higher image resolution than conventional fluorescence microscopy, and in the meantime acquires each snapshot more slowly, this paradox puts a more stringent constraint on the motion of the cellular structure.

6.5 Photo- and Chemical Toxicity

Live-cell super-resolution imaging typically requires stronger excitation light intensity than conventional microscopy. In some cases, chemical additives are also added in the imaging buffer to facilitate photoswitching of fluorophores. These conditions can affect cell viability. Red or near-infrared light is less phototoxic than blue or UV light and is thus preferred for live-cell imaging. Some photoswitchable organic dyes, including Cy5, Alexa 647, Cy7, and Alexa 750 can be imaged at far-red and near-infrared wavelengths [18, 40]. Recently, an orange-to-far-red photoswitchable fluorescent protein was also developed [96]. In addition to the imaging laser, UV or violet light is often used for activating photoswitchable dyes and fluorescent proteins. Coupling activator dyes with photoswitchable reporter dyes can help to reduce the activation intensity or to change the activation color to a less phototoxic wavelength. To prolong the lifetime of fluorophores, the imaging medium is often supplemented with oxygen and/or radical scavengers, which are also widely used for conventional live-cell imaging [97]. In addition, some organic dyes perform better in the presence of thiols or reducing/oxidizing agents. Although when added at low concentrations, these additives do not affect cell health, they have the potential to perturb the dynamics of interest and the viability of live cells at high concentrations. Hence, control experiments to test whether the imaging conditions perturb the cell viability and the dynamics under investigation are necessary.

7 Choice of Fluorescent Probes

As discussed above, the implementation of STORM, (F)PALM, and related methods depends on the stochastic switching of the fluorescent probes between the dark and emitting states. In an effort to provide general guidelines for the characterization of super-resolution probes, a recent study systematically investigated the properties of 26 organic dyes and identified several parameters as being crucial in determining the quality of the final super-resolution images: (1) photons per switching event, (2) on-off contrast ratio, (3) on-off duty cycle, and (4) number of switching cycles [40]. An ideal probe should emit a large number of photons per switching cycle and should provide high contrast between the on and off states, i.e., give bright emission in the emitting state (to maximize signal) and negligible emission in the dark state (to minimize background), so as to maximize the localization precision. It should also have a low on-off duty cycle, defined as the fraction of time that the probe spends in the on state, to maximize the number of probe molecules that can be localized per diffraction-limited volume. Together, these factors ensure a high overall image resolution when both localization precision and localization densities are considered. In addition, probes with a large number of switching cycles allow many super-resolution snapshots to be taken, which greatly benefit imaging of dynamic processes. Finally, other factors, including physical size of the probe and how the sample will be labeled with the probe, should also be taken into consideration when designing experiments.

Several subsequent chapters in this book are dedicated to probe development for nanoscopy. Here we only provide a general overview and briefly discuss the advantages and disadvantages of different types of probes for super-resolution applications.

7.1 Fluorescent Dyes vs. Fluorescent Proteins

Some photoswitchable dyes have excellent brightness (defined here as the number of photons detected per switching cycle), high contrast ratio, and low on-off duty ratio. Among the tens of synthesized dyes that have been tested, the red-absorbing (640–700 nm) dyes, Cy5, Alexa 647, and Dyomics 654 are among the best probes, each providing ~5,000 detected photons per switching cycle, exhibiting undetectable dark state fluorescence, and have an on-off duty ratio of ~0.001 or lower [40]. They consistently give higher-quality images than other probes. For multicolor imaging (see Sect. 5.2), dyes with reasonably good performance have also been identified for other spectral ranges; i.e., blue dyes Atto488 and Alexa 488; yellow dye Cy3B; and near-infrared dyes (740–805 nm) DyLight 750, Cy7, and Alexa Fluor 750 [40].

A popular way to label cellular structures with dyes is through immunofluorescence, either directly with dye-labeled primary antibodies or indirectly with labeled secondary antibodies. An advantage of the immunofluorescence scheme is that it

allows endogenous proteins to be labeled without introducing fusion proteins, which could potentially perturb the localization, function, and expression level of the target proteins. The drawbacks are that antibodies are relatively bulky (~10 nm in size) and it is difficult to label proteins in live cells with antibodies. These problems can be at least partially overcome through alternative dye-labeling methods. In hybrid fusion approaches, a specific enzyme or peptide tag is genetically fused to the protein of interest and the dye molecules are specifically attached to the tags [41, 77, 86–88, 98, 99]. In particular, short-peptide tagging methods like sortagging [100] and LplA labeling [101, 102] could be especially beneficial due to their small sizes (~1–2 nm). Target-specific small molecules can also be used to label cellular structures in some cases, e.g., phalloidin specifically labels filamentous actin [53].

Another popular type of fluorescent probes is fluorescent proteins. Compared to organic dyes, the advantage of fluorescent proteins is that they can be genetically fused to target protein of interest, offering a convenient and powerful way to label proteins in live cells. One should, however, be cautious about the potential artifacts on protein localization and function induced by fluorescent protein tags, which are ~4 nm in size and tend to oligomerize. Overexpression of the fusion proteins may also cause artifacts. The main disadvantage of fluorescent proteins is their inferior photophysical properties as compared to dyes. Fluorescent proteins are generally dimmer than organic dyes. The bright photoswitchable/photoactivable fluorescent proteins, such as Dendra2 [80], mEos2 [81], PAmCherry [73], and PAtagRFP [82] provide ~1,000 detected photons per switching cycles. The dark states of fluorescent proteins also tend to have non-negligible fluorescence, providing lower contrast ratio than switchable dyes. The on-off duty cycle of these fluorescent proteins, however, can be as low as 10^{-4}–10^{-5}, which is better than that of most organic dyes.

In addition to dyes and fluorescent proteins, quantum dots have also been used for super-resolution imaging [103].

7.2 Dye Pairs vs. Single Dyes

It has been shown that highly controllable photoswitches can be constructed when a photoswitchable reporter dye molecule (e.g., Cy5) is brought into the proximity of another activator dye molecule (e.g., Cy3) [104]. In this scheme, the reporter dye is imaged and switched off by the excitation light, while the activator dye is capable of activating the reporter when illuminated by light that matches the activator's absorption spectrum. The presence of the activator dye greatly facilitates the activation process and uniquely enables activation-based multicolor imaging, where activator dyes with different absorption spectra are used (more details of this multicolor imaging scheme are described in Sect. 5.1) [18]. For immunofluorescence imaging, antibodies can be nonspecifically labeled with both activator and reporter dyes in a single reaction step, in ways similar to labeling antibodies with a single type of dye. However, when labeling with the hybrid fusion approaches using

protein or peptide tags, covalently linked activator-reporter dye pairs are required. Such pre-linked dye pairs have been synthesized [62, 105].

The photoswitchable reporter dyes can also be directly activated through either the excitation light or an additional short-wavelength (e.g., UV to green) light [23, 68]. The major advantage of using the reporter dye alone (as opposed to dye pairs) is that a single dye can be more easily used to directly label target proteins (such as through the hybrid fusion approach) or to label small molecules. However, in the absence of an activator dye, the light intensity used to activate the reporter dye is often several orders of magnitude higher than when the activator dye is present. Strong short-wavelength illuminations, particularly UV and violet, could induce phototoxicity. Multicolor imaging with single dyes can be accomplished through the emission-based multicolor scheme. The advantages and disadvantages of the activation- and emission-based multicolor schemes are described in Sect. 5.

7.3 Reversible Photoswitchable vs. Irreversible Photoactivatable Probes

The switchable probes used for super-resolution imaging can also be categorized according to their switching properties. The reversible, *photoswitchable* probes can be switched between the emitting and dark states multiple times. An advantage of using reversible, photoswitchable probes is that each probe can be localized multiple times. This is particularly useful for live-cell studies, in which the morphological changes of structures often need to be tracked over a substantially long period. In addition, most photoswitchable probes start in an emitting state before being switched off prior to super-resolution imaging. Conventional fluorescence images can thus be obtained before super-resolution imaging is performed, which in practice is useful for locating regions of interest.

In comparison, the irreversible, *photoactivatable* probes can only be brought into the emission state once. During imaging, individual probes are activated, imaged, and permanently photobleached. As each probe can only be imaged once, these probes are less suitable for monitoring live-cell dynamics that requires many snapshots. On the other hand, the fact that each molecule only appears once makes it easier to quantify the number of molecules in a target structure. It is worth noting though, many photoactivatable fluorescent proteins that are thought to be irreversibly activated can in fact be switched on and off a few times [106, 107], and methods to account for this reversible blinking effect in protein quantification have been recently developed [95, 108, 109]. For stoichiometric quantification, one also needs to know the fraction of target molecules that are labeled and the fraction of the fluorescent labels that have matured (for fluorescent proteins) and can be photoactivated (for both fluorescent proteins and dyes).

Rather than switching between a dark state and an emitting state, *photochromic* probes switch from one emitting color to a different color (e.g., from green to red)

upon being activated by light. For example, EosFP switches from a green, pre-activation state to an orange/red, post-activation state [110]. Photochromic probes can either irreversibly or reversibly switch between two emitting states. Photochromic probes, in general, also allow for the recording of conventional fluorescence images before super-resolution imaging, e.g., in the color channel before photoswitching.

7.4 Other Probes

Beyond using photoswitchable fluorescent probes as discussed above, it is also worth mentioning that alternative strategies have also been developed. These strategies include the use of the PAINT approach [28], in which the emission of the probes is recorded when they stochastically bind to the target, and the reversible chemical quenchers [29], in which the stochastic switching of probes is realized through the reversible binding of fluorescence quenchers (Sect. 2).

8 Applications

Due to their superb resolving power and relatively simple implementation, STORM, (F)PALM, and related methods have been rapidly adopted by many labs and applied to a variety of biological systems. Here we will focus on applications in our laboratory and related studies. Interested readers can also find numerous applications in other chapters of this book.

8.1 Applications in Cell Biology

In eukaryotic cells, many well-characterized structures such as the cytoskeleton and other protein scaffolds have been reexamined with super-resolution fluorescence microscopy. These proof-of-principle systems not only demonstrated the resolving power of the technique but also gave a glimpse of its potential for novel discoveries. One application where this potential has been demonstrated is the study of clathrin-coated pits, an essential cellular structure used for receptor-mediated endocytosis. A clathrin-coated pit on the plasma membrane contains layers of receptor and adaptor proteins under the clathrin coat, forming a spherical shell with a diameter of ~100 nm. The sub-diffraction-limit morphology of clathrin-coated pits was used to demonstrate the multicolor [18], 3D [39], and live-cell [41] capabilities of STORM imaging in cells. In an in vitro model system, two membrane-curvature generating/sensing proteins, dynamin and FBP17, were found to distribute differentially on membrane tubules connecting clathrin-coated

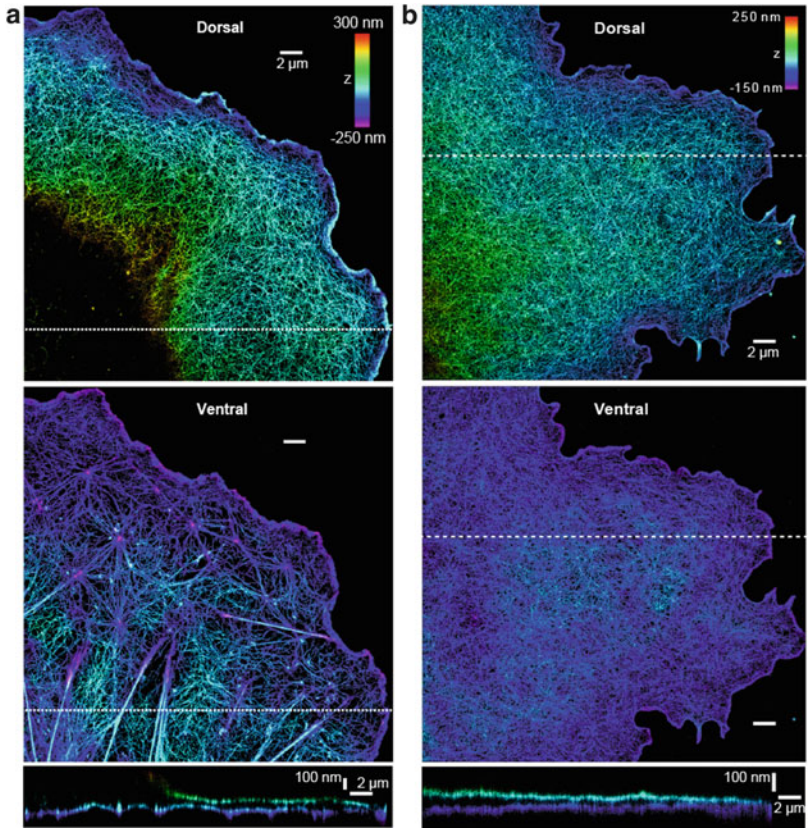

Fig. 7 STORM images of actin in sheet-like protrusions. (**a**) Dorsal (*top*) and ventral (*middle*) actin layers of a BS-C-1 cell. *Bottom panel*: Vertical cross section (500 nm wide in *y*) along the dotted lines in the *top* and *middle panels*. (**b**) Dorsal (*top*) and ventral (*middle*) actin layers of a COS-7 cell treated with blebbistatin, an inhibitor for myosin II. *Bottom panel*: Vertical cross section (500 nm wide in y) along the dashed lines in the top and middle panels. Scale bars: 2 μm (*horizontal*), 100 nm (*vertical*). Figure adapted from reference [53]

pits: While FBP17 coats the entire tubule below the clathrin-coated pit, dynamin is only located at the narrow neck region between the clathrin-coated pit and the FBP-17-coated tubule [111]. In conjunction with confocal fluorescence imaging and electron microscopy, STORM revealed an unexpected role of FBP17 in creating endocytic vesicles [111].

Actin cytoskeleton is another representative example. Dual-objective STORM resolved individual actin filaments in cells and revealed 3D ultrastructure of the actin cytoskeleton [53]. In particular, two vertically separated layers of actin networks were revealed in sheet-like cell protrusions (Fig. 7a). The two actin layers exhibited highly distinct structural organizations: The dorsal layer appeared as a consistently dense and homogeneous meshwork; the ventral layer typically formed

a web-like structure with a lower filament density and highly variable organization (Fig. 7a). This striking structural difference between the ventral and dorsal actin networks could be completely removed by inhibiting myosin II activity (Fig. 7b), suggesting an important role of myosin II in maintaining the distinct structural organization of the two actin networks.

8.2 Applications in Microbiology

In addition to eukaryotic cells, super-resolution fluorescence microscopy is also becoming an important imaging tool for investigating bacteria. Due to the very small volumes (~1 μm^3) of prokaryotic cells, it is difficult to resolve the subcellular organization of bacteria using conventional fluorescence microscopy. Ultrastructural studies have thus mostly relied on electron microscopy (EM). However, it is often difficult to resolve molecule-specific structures in EM images due to poor molecular contrast. Moreover, EM cannot be used to image live specimens and monitor dynamics. Fluorescence imaging methods with molecule-specific contrast and nanometer-scale resolution promise to change our view of bacterial cell biology by revealing how proteins are organized in bacterial cells. For example, clustered distribution of chemotaxis proteins, Tar receptor, CheY, and CheW has been observed in fixed *E. coli* cells [112]. A helical organization of MreB, an actin analog, has been observed in live *Caulobacter crescentus* [27]. The DNA-partitioning proteins, ParA and ParB, form narrow, linear polymer structures in *Caulobacter crescentus*, resembling mitotic spindles in eukaryotic cells [113]. A major nucleoid-associated protein (NAP), H-NS, forms tight clusters in the nucleoid in live *E. coli* cells, ~ 2 clusters per chromosome (Fig. 8a) [114]. This clustered distribution, highly distinct from other major NAPs (Fig. 8b), is formed due to the self-interactions between the N-terminal domain of H-NS. As a global transcriptional silencer, H-NS sequester numerous H-NS–regulated genes into these compact clusters (Fig. 8c), which serve as organization centers to organize bacterial chromosome. Other bacterial proteins, such as HU, IHF, FIS, StpA [114, 115], FtsZ [116], and SpoIIIE [117], have also been investigated using super-resolution imaging.

8.3 Applications in Neurobiology

Another exciting area into which super-resolution imaging will likely bring new breakthroughs is neurobiology. Neurons have complex, multi-scale morphologies. Many important neuronal structures have dimensions on submicron or nanometer scales. For example, axons in the neuropil can be as thin as 100 nm. Dendritic spine necks are often narrower than 100 nm. Chemical synapses, the basic functional units in the brain that mediate neurotransmitter-based communications between

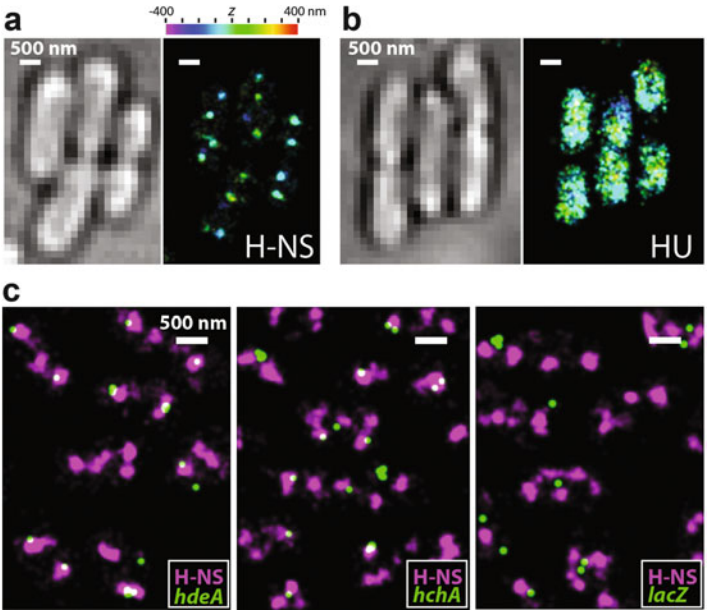

Fig. 8 STORM images of nucleoid-associated proteins in living *E. coli* cells. (**a**) H-NS forms compact clusters in the nucleosome. *Left panel*: Bright-field image of the cells. *Right panel*: 3D super-resolution image of H-NS fused with mEos2. The z-coordinates are color coded according to the color bar (*top*). (**b**) HU is scattered through the nucleoid. *Left panel*: Bright-field image of the cells. *Right panel*: 3D super-resolution image of HU fused with mEos2. (**c**) Colocalization of H-NS clusters and gene loci revealed by two-color live-cell images of mEos2-labeled H-NS (*magenta*) and eYFP-labeled gene loci (*green*). The two H-NS–regulated loci, *hdeA* (*left*) and *hchA* (*center*), were colocalized with H-NS clusters to a noticeably larger extent than did *lacZ* (*right*), which is not regulated by H-NS. Scale bars: 500 nm. Figure adapted from reference [114]

neurons and their target cells, are typically several hundred nanometers in size. Hence, both the investigations of sub-neuronal structures and the mapping of neural connectivity in the brain require imaging tools with nanometer resolution. Indeed, super-resolution fluorescence imaging has begun to provide new insights into neuronal and sub-neuronal structures. For example, multicolor 3D super-resolution imaging has been performed to determine the molecular distributions of ten protein components of the presynaptic active zone and the postsynaptic density (Fig. 9) [70]. This study has shown a laminar organization of the postsynaptic density components, PSD-95, Shank, and Homer, consistent with previous EM analysis [118] (Fig. 9i). It has also revealed a previously unknown, oriented organization of the presynaptic scaffolding proteins, Bassoon and Piccolo (Fig. 9i). Significant variations in the spatial distributions of neurotransmitter receptors have also been observed from synapse to synapse (Fig. 9f–h). Moreover, quantitative receptor composition analysis led to the discovery of a surprisingly large population of immature synapses with activity-dependent plasticity in the adult accessory olfactory bulb [70]. In a different study, high-density single-molecule tracking with

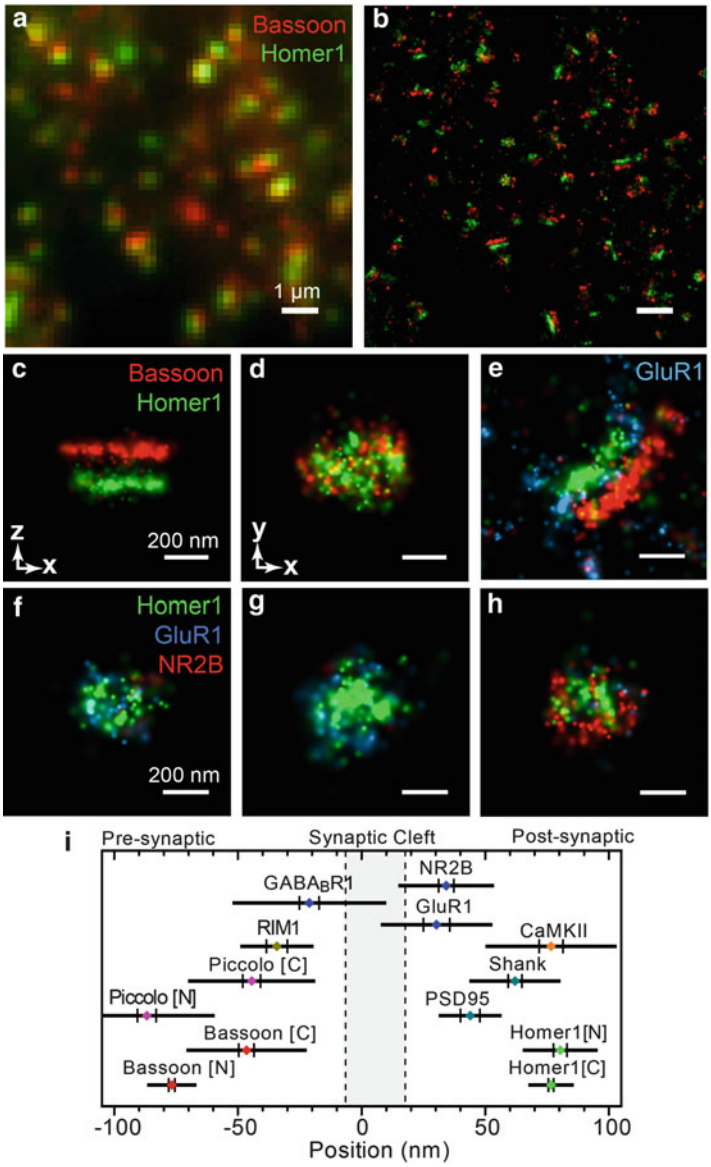

Fig. 9 STORM images of synaptic proteins in brain tissues. (**a**–**d**) STORM imaging of pre- and postsynaptic scaffolding proteins. Presynaptic protein Bassoon (*red*) and postsynaptic protein Homer1 (*green*) in the mouse main olfactory bulb were immunolabeled with Cy3-Alexa 647 and Alexa 405-Alexa 647 dye pairs. Partially overlapping puncta in a conventional image (**a**) were clearly resolved as distinct synaptic structures in the corresponding STORM image (**b**). (**c**, **d**) Well-separated elliptical disks of presynaptic scaffolds Bassoon (*red*) and postsynaptic scaffolds Homer1 (*green*) are shown in two different orientations. (**c**) A side view with the trans-synaptic axis rotated into the viewing plane. (**d**) An en face view with the trans-synaptic axis rotated

photoactivatable proteins has been used to investigate actin dynamics within dendritic spines [119]. This work has revealed a heterogeneous distribution of the actin polymerization rate as well as highly localized but spatially diverse foci of actin polymerization, indicating an active regulatory role of actin in the synapses [119].

Due to the space limit, we could only provide a glimpse of the recent applications of STORM, (F)PALM, and related imaging methods. More applications of these methods can be found in subsequent chapters of this book. The number of applications is increasing exponentially. We expect numerous new discoveries enabled by these powerful imaging approaches.

9 Concluding Remarks and Future Developments

By separating the otherwise spatially overlapping fluorescence signals from densely packed fluorophores in the time domain, STORM, (F)PALM, and related methods overcome the diffraction limit through switching and localization of individual molecules. These methods improve the spatial resolution of far-field optical microscopy by more than an order of magnitude, achieving resolutions down to the sub-10 nm range for biological specimens. The ability to perform multicolor, 3D, and live-cell imaging further enhances the versatility of these methods. Super-resolution fluorescence imaging can also be combined with other microscopy methods, such as EM [16, 120], to simultaneously exploit the respective strengths of different imaging modalities.

In principle, the image resolution of these methods can be extremely high, as long as suitable conditions could be found to allow for both maximal emission of photons and proper photoswitching (though in practice, being a fluorescence imaging modality, the image resolution may not exceed the size of the fluorescent labels). It is thus expected that the spatial resolution of these methods could become substantially better than 10 nm. In fact, a recent work has demonstrated the use of reductive caging to generate ultrabright photoactivatable fluorescent probes and improved image resolution to the single digit nanometer range [121]. We anticipate even higher resolution to be possible. Likewise, further improvement in faster switching probes, faster camera, and image analysis algorithms should also allow

Fig. 9 (continued) perpendicular to the viewing plane. (**e**) AMPA receptor subunit GluR1 (*blue*) imaged together with Bassoon (*red*) and Homer1 (*green*). A side view of a synapse is shown here. (**f–h**) Radial distributions of glutamate neurotransmitter receptors in the postsynaptic density (PSD) shown in the en face view. AMPA receptor subunit GluR1 (*blue*) and NMDA receptor subunit NR2B (*red*) were imaged together with Homer1 (*green*). (**i**) Axial positions of 13 synaptic proteins along the trans-synaptic axis. For each protein, the *colored dots* indicate the mean position, the two vertical lines represent the associated standard error, and the half-lengths of the horizontal bar denote standard deviation, derived from multiple synapses. Scale bars: 1 μm (**a–b**), 200 nm (**c–h**). Figure adapted from reference [70]

imaging with time resolutions substantially faster than 1 s. Another important frontier is in vivo imaging, which requires substantial improvement of the imaging depth of these methods in scattering tissues.

Future development of these methods will require synergy between multiple disciplines. On the optics and hardware front, careful design and/or calibration of the imaging setup [6] could lead to extraordinarily high localization precision of single molecules. Besides continued innovations in the detection paths [39, 53–57, 59, 61, 122], recent studies have shown that developments in the illumination paths are also fruitful, especially for increasing imaging depth using multi-photoactivation and sheet illumination [65, 67]. Advances in cameras (e.g., scientific CMOS) [123, 124] could also be beneficial by improving the spatiotemporal resolution and/or introducing new capabilities.

Meanwhile, developments in analysis algorithms and theoretical modeling, possibly in combination with modifications to how the experimental data are acquired, could continue to improve the performance of these super-resolution methods and further broaden their range of application. For example, for improvement of spatial resolution, maximum-likelihood fitting of single-molecule images to true PSFs has led to more optimal localization results [125, 126]. For improvement of temporal resolution, methods have been developed to analyze overlapped images of multiple fluorophores simultaneously [30–33, 36–38] (see also discussion in Sects. 2 and 6.2).

On the chemistry and chemical biology side, the design and/or screening of new photoswitchable probes [40, 84, 85, 127, 128] with superior brightness of the fluorescent state (i.e., large number of photons per switching event), higher contrast ratio between the fluorescent and dark state, lower on-off duty cycle, faster switching speed, and more switching cycles would be tremendously helpful not only for improving the spatial and temporal resolutions, but also for prolonging the observation time window and expanding the color palette. To this end, understanding the photoswitching mechanisms of the probes will be very useful [128–131]. Novel stochastic readouts other than photoswitching could further expand the palette of probes and the information content [28, 29, 132]. The development of new, live-cell-compatible labeling methods that can achieve high molecular specificity and high labeling density with small label sizes [98] would also contribute substantially to further improvement of imaging qualities.

Combining the above efforts, we anticipate that true molecular-scale resolution in living cells, tissues, and even living animals will be within reach some day. At the other end of the spectrum, engineering efforts have packaged the imaging system into a compact, easy-to-operate unit. Commercial, user-friendly, super-resolution imaging systems are becoming available through multiple companies [133, 134]. These systems could make the benefits of these imaging methods accessible to all researchers, not just those who are comfortable with building their own setups.

Acknowledgments We thank Hazen P. Babcock for help in manuscript preparation. This work is supported in part by the National Institute of Health (to X.Z.). X.Z. is a Howard Hughes Medical Institute investigator.

References

1. Guilford WH, Cheezum MK, Walker WF (2001) Quantitative comparison of algorithms for tracking single fluorescent particles. Biophys J 81(4):2378–2388
2. Thompson RE, Larson DR, Webb WW (2002) Precise nanometer localization analysis for individual fluorescent probes. Biophys J 82(5):2775–2783
3. Gelles J, Schnapp BJ, Sheetz MP (1988) Tracking kinesin-driven movements with nanometre-scale precision. Nature 331(6155):450–453
4. Moerner WE, Orrit M (1999) Illuminating single molecules in condensed matter. Science 283(5408):1670–1676
5. Yildiz A, Forkey JN, McKinney SA, Ha T, Goldman YE, Selvin PR (2003) Myosin V walks hand-over-hand: single fluorophore imaging with 1.5-nm localization. Science 300(5628):2061–2065
6. Pertsinidis A, Zhang YX, Chu S (2010) Subnanometre single-molecule localization, registration and distance measurements. Nature 466(7306):647–651
7. Betzig E (1995) Proposed method for molecular optical imaging. Opt Lett 20(3):237–239
8. Schmidt J, van Oijen AM, Kohler J, Muller M, Brakenhoff GJ (1998) 3-Dimensional super-resolution by spectrally selective imaging. Chem Phys Lett 292(1–2):183–187
9. Lacoste TD, Michalet X, Pinaud F, Chemla DS, Alivisatos AP, Weiss S (2000) Ultrahigh-resolution multicolor colocalization of single fluorescent probes. Proc Natl Acad Sci U S A 97(17):9461–9466
10. Churchman LS, Okten Z, Rock RS, Dawson JF, Spudich JA (2005) Single molecule high-resolution colocalization of Cy3 and Cy5 attached to macromolecules measures intramolecular distances through time. Proc Natl Acad Sci U S A 102(5):1419–1423
11. Gordon MP, Ha T, Selvin PR (2004) Single-molecule high-resolution imaging with photobleaching. Proc Natl Acad Sci U S A 101(17):6462–6465
12. Qu XH, Wu D, Mets L, Scherer NF (2004) Nanometer-localized multiple single-molecule fluorescence microscopy. Proc Natl Acad Sci U S A 101(31):11298–11303
13. Lidke KA, Rieger B, Jovin TM, Heintzmann R (2005) Superresolution by localization of quantum dots using blinking statistics. Opt Express 13(18):7052–7062
14. Lagerholm BC, Averett L, Weinreb GE, Jacobson K, Thompson NL (2006) Analysis method for measuring submicroscopic distances with blinking quantum dots. Biophys J 91(8):3050–3060
15. Rust MJ, Bates M, Zhuang XW (2006) Sub-diffraction-limit imaging by stochastic optical reconstruction microscopy (STORM). Nat Methods 3(10):793–795
16. Betzig E, Patterson GH, Sougrat R, Lindwasser OW, Olenych S, Bonifacino JS, Davidson MW, Lippincott-Schwartz J, Hess HF (2006) Imaging intracellular fluorescent proteins at nanometer resolution. Science 313(5793):1642–1645
17. Hess ST, Girirajan TPK, Mason MD (2006) Ultra-high resolution imaging by fluorescence photoactivation localization microscopy. Biophys J 91(11):4258–4272
18. Bates M, Huang B, Dempsey GT, Zhuang XW (2007) Multicolor super-resolution imaging with photo-switchable fluorescent probes. Science 317(5845):1749–1753
19. Huang B, Babcock H, Zhuang XW (2010) Breaking the diffraction barrier: super-resolution imaging of cells. Cell 143(7):1047–1058
20. Egner A, Geisler C, Von Middendorff C, Bock H, Wenzel D, Medda R, Andresen M, Stiel AC, Jakobs S, Eggeling C, Schonle A, Hell SW (2007) Fluorescence nanoscopy in whole cells by asynchronous localization of photoswitching emitters. Biophys J 93(9):3285–3290
21. Bock H, Geisler C, Wurm CA, Von Middendorff C, Jakobs S, Schonle A, Egner A, Hell SW, Eggeling C (2007) Two-color far-field fluorescence nanoscopy based on photoswitchable emitters. Appl Phys B-Lasers Opt 88(2):161–165
22. Folling J, Bossi M, Bock H, Medda R, Wurm CA, Hein B, Jakobs S, Eggeling C, Hell SW (2008) Fluorescence nanoscopy by ground-state depletion and single-molecule return. Nat Methods 5(11):943–945

23. Heilemann M, van de Linde S, Schuttpelz M, Kasper R, Seefeldt B, Mukherjee A, Tinnefeld P, Sauer M (2008) Subdiffraction-resolution fluorescence imaging with conventional fluorescent probes. Angew Chem-Int Edit 47(33):6172–6176
24. Vogelsang J, Cordes T, Forthmann C, Steinhauer C, Tinnefeld P (2009) Controlling the fluorescence of ordinary oxazine dyes for single-molecule switching and superresolution microscopy. Proc Natl Acad Sci U S A 106(20):8107–8112
25. Lemmer P, Gunkel M, Weiland Y, Muller P, Baddeley D, Kaufmann R, Urich A, Eipel H, Amberger R, Hausmann M, Cremer C (2009) Using conventional fluorescent markers for far-field fluorescence localization nanoscopy allows resolution in the 10-nm range. J Microsc-Oxf 235(2):163–171
26. Dickson RM, Cubitt AB, Tsien RY, Moerner WE (1997) On/off blinking and switching behaviour of single molecules of green fluorescent protein. Nature 388(6640):355–358
27. Biteen JS, Thompson MA, Tselentis NK, Bowman GR, Shapiro L, Moerner WE (2008) Super-resolution imaging in live *Caulobacter crescentus* cells using photoswitchable EYFP. Nat Methods 5(11):947–949
28. Sharonov A, Hochstrasser RM (2006) Wide-field subdiffraction imaging by accumulated binding of diffusing probes. Proc Natl Acad Sci U S A 103(50):18911–18916
29. Schwering M, Kiel A, Kurz A, Lymperopoulos K, Sprodefeld A, Kramer R, Herten DP (2011) Far-field nanoscopy with reversible chemical reactions. Angew Chem-Int Edit 50(13):2940–2945
30. Holden SJ, Uphoff S, Kapanidis AN (2011) DAOSTORM: an algorithm for high-density super-resolution microscopy. Nat Methods 8(4):279–280
31. Huang F, Schwartz SL, Byars JM, Lidke KA (2011) Simultaneous multiple-emitter fitting for single molecule super-resolution imaging. Biomed Opt Express 2(5):1377–1393
32. Babcock H, Sigal Y, Zhuang X (2012) A high-density 3D localization algorithm for stochastic optical reconstruction microscopy. Optical Nanoscopy 1(1):6
33. Zhu L, Zhang W, Elnatan D, Huang B (2012) Faster STORM using compressed sensing. Nat Methods 9(7):721–723
34. Burnette DT, Sengupta P, Dai YH, Lippincott-Schwartz J, Kachar B (2011) Bleaching/blinking assisted localization microscopy for superresolution imaging using standard fluorescent molecules. Proc Natl Acad Sci U S A 108(52):21081–21086
35. Simonson PD, Rothenberg E, Selvin PR (2011) Single-molecule-based super-resolution images in the presence of multiple fluorophores. Nano Lett 11(11):5090–5096
36. Cox S, Rosten E, Monypenny J, Jovanovic-Talisman T, Burnette DT, Lippincott-Schwartz J, Jones GE, Heintzmann R (2012) Bayesian localization microscopy reveals nanoscale podosome dynamics. Nat Methods 9(2):195–200
37. Dertinger T, Colyer R, Iyer G, Weiss S, Enderlein J (2009) Fast, background-free, 3D super-resolution optical fluctuation imaging (SOFI). Proc Natl Acad Sci U S A 106(52):22287–22292
38. Mukamel E, Babcock H, Zhuang X (2012) Statistical deconvolution for superresolution fluorescence microscopy. Biophys J 102(10):2391–2400
39. Huang B, Wang WQ, Bates M, Zhuang XW (2008) Three-dimensional super-resolution imaging by stochastic optical reconstruction microscopy. Science 319(5864):810–813
40. Dempsey GT, Vaughan JC, Chen KH, Bates M, Zhuang X (2011) Evaluation of fluorophores for optimal performance in localization-based super-resolution imaging. Nat Methods 8(12):1027–1036
41. Jones SA, Shim SH, He J, Zhuang XW (2011) Fast, three-dimensional super-resolution imaging of live cells. Nat Methods 8(6):499–505
42. Shroff H, Galbraith CG, Galbraith JA, Betzig E (2008) Live-cell photoactivated localization microscopy of nanoscale adhesion dynamics. Nat Methods 5(5):417–423
43. Kao HP, Verkman AS (1994) Tracking of single fluorescent particles in three dimensions: use of cylindrical optics to encode particle position. Biophys J 67(3):1291–1300
44. van Oijen AM, Kohler J, Schmidt J, Muller M, Brakenhoff GJ (1998) 3-Dimensional super-resolution by spectrally selective imaging. Chem Phys Lett 292(1–2):183–187

45. Speidel M, Jonas A, Florin EL (2003) Three-dimensional tracking of fluorescent nanoparticles with subnanometer precision by use of off-focus imaging. Opt Lett 28(2):69–71
46. Prabhat P, Ram S, Ward ES, Ober RJ (2006) Simultaneous imaging of several focal planes in fluorescence microscopy for the study of cellular dynamics in 3D. Proc SPIE 6090:60900L
47. Holtzer L, Meckel T, Schmidt T (2007) Nanometric three-dimensional tracking of individual quantum dots in cells. Appl Phys Lett 90(5):3
48. Toprak E, Balci H, Blehm BH, Selvin PR (2007) Three-dimensional particle tracking via bifocal imaging. Nano Lett 7(7):2043–2045
49. Pavani SRP, Piestun R (2008) Three dimensional tracking of fluorescent microparticles using a photon-limited double-helix response system. Opt Express 16(26):22048–22057
50. Braun D, Fromherz P (1998) Fluorescence interferometry of neuronal cell adhesion on microstructured silicon. Phys Rev Lett 81(23):5241–5244
51. Bilenca A, Cao J, Colice M, Ozcan A, Bouma B, Raftery L, Tearney G (2008) Fluorescence interferometry: principles and applications in biology. Ann N Y Acad Sci 1130(1):68–77
52. McMahon MD, Berglund AJ, Carmichael P, McClelland JJ, Liddle JA (2009) 3D particle trajectories observed by orthogonal tracking microscopy. ACS Nano 3(3):609–614
53. Xu K, Babcock HP, Zhuang X (2012) Dual-objective STORM reveals three-dimensional filament organization in the actin cytoskeleton. Nat Methods 9(2):185–188
54. Juette MF, Gould TJ, Lessard MD, Mlodzianoski MJ, Nagpure BS, Bennett BT, Hess ST, Bewersdorf J (2008) Three-dimensional sub-100 nm resolution fluorescence microscopy of thick samples. Nat Methods 5(6):527–529
55. Pavani SRP, Thompson MA, Biteen JS, Lord SJ, Liu N, Twieg RJ, Piestun R, Moerner WE (2009) Three-dimensional, single-molecule fluorescence imaging beyond the diffraction limit by using a double-helix point spread function. Proc Natl Acad Sci U S A 106(9):2995–2999
56. Lew MD, Lee SF, Badieirostami M, Moerner WE (2011) Corkscrew point spread function for far-field three-dimensional nanoscale localization of pointlike objects. Opt Lett 36(2):202–204
57. Shtengel G, Galbraith JA, Galbraith CG, Lippincott-Schwartz J, Gillette JM, Manley S, Sougrat R, Waterman CM, Kanchanawong P, Davidson MW, Fetter RD, Hess HF (2009) Interferometric fluorescent super-resolution microscopy resolves 3D cellular ultrastructure. Proc Natl Acad Sci U S A 106(9):3125–3130
58. Von Middendorff C, Egner A, Geisler C, Hell S, Schonle A (2008) Isotropic 3D Nanoscopy based on single emitter switching. Opt Express 16(25):20774–20788
59. Aquino D, Schonle A, Geisler C, von Middendorff C, Wurm CA, Okamura Y, Lang T, Hell SW, Egner A (2011) Two-color nanoscopy of three-dimensional volumes by 4Pi detection of stochastically switched fluorophores. Nat Methods 8(4):353–359
60. Lew MD, Lee SF, Ptacin JL, Lee MK, Twieg RJ, Shapiro L, Moerner WE (2011) Three-dimensional superresolution colocalization of intracellular protein superstructures and the cell surface in live *Caulobacter crescentus*. Proc Natl Acad Sci U S A 108(46):E1102–E1110
61. Tang JY, Akerboom J, Vaziri A, Looger LL, Shank CV (2010) Near-isotropic 3D optical nanoscopy with photon-limited chromophores. Proc Natl Acad Sci U S A 107(22):10068–10073
62. Huang B, Jones SA, Brandenburg B, Zhuang XW (2008) Whole-cell 3D STORM reveals interactions between cellular structures with nanometer-scale resolution. Nat Methods 5(12):1047–1052
63. Vaziri AVA, Tang JY, Shroff H, Shank CV (2008) Multilayer three-dimensional super resolution imaging of thick biological samples. Proc Natl Acad Sci U S A 105(51):20221–20226
64. Folling J, Belov V, Kunetsky R, Medda R, Schonle A, Egner A, Eggeling C, Bossi M, Hell SW (2007) Photochromic rhodamines provide nanoscopy with optical sectioning. Angew Chem-Int Edit 46(33):6266–6270

65. York AG, Ghitani A, Vaziri A, Davidson MW, Shroff H (2011) Confined activation and subdiffractive localization enables whole-cell PALM with genetically expressed probes. Nat Methods 8(4):327–333
66. Huisken J, Swoger J, Del Bene F, Wittbrodt J, Stelzer EH (2004) Optical sectioning deep inside live embryos by selective plane illumination microscopy. Science 305(5686):1007–1009
67. Cella Zanacchi F, Lavagnino Z, Perrone Donnorso M, Del Bue A, Furia L, Faretta M, Diaspro A (2011) Live-cell 3D super-resolution imaging in thick biological samples. Nat Methods 8(12):1047–1049
68. Zhuang XW (2009) Nano-imaging with STORM. Nat Photonics 3(7):365–367
69. Bates M, Dempsey GT, Chen KH, Zhuang X (2012) Multicolor super-resolution fluorescence imaging via multi-parameter fluorophore detection. ChemPhysChem 13(1):99–107
70. Dani A, Huang B, Bergan J, Dulac C, Zhuang XW (2010) Superresolution imaging of chemical synapses in the brain. Neuron 68(5):843–856
71. Shroff H, Galbraith CG, Galbraith JA, White H, Gillette J, Olenych S, Davidson MW, Betzig E (2007) Dual-color superresolution imaging of genetically expressed probes within individual adhesion complexes. Proc Natl Acad Sci U S A 104(51):20308–20313
72. Andresen M, Stiel AC, Folling J, Wenzel D, Schonle A, Egner A, Eggeling C, Hell SW, Jakobs S (2008) Photoswitchable fluorescent proteins enable monochromatic multilabel imaging and dual color fluorescence nanoscopy. Nat Biotechnol 26(9):1035–1040
73. Subach FV, Patterson GH, Manley S, Gillette JM, Lippincott-Schwartz J, Verkhusha VV (2009) Photoactivatable mCherry for high-resolution two-color fluorescence microscopy. Nat Methods 6(2):153–159
74. Gunewardene MS, Subach FV, Gould TJ, Penoncello GP, Gudheti MV, Verkhusha VV, Hess ST (2011) Superresolution imaging of multiple fluorescent proteins with highly overlapping emission spectra in living cells. Biophys J 101(6):1522–1528
75. Bossi M, Folling J, Belov VN, Boyarskiy VP, Medda R, Egner A, Eggeling C, Schonle A, Hell SW (2008) Multicolor far-field fluorescence nanoscopy through isolated detection of distinct molecular species. Nano Lett 8(8):2463–2468
76. van de Linde S, Endesfelder U, Mukherjee A, Schuttpelz M, Wiebusch G, Wolter S, Heilemann M, Sauer M (2009) Multicolor photoswitching microscopy for subdiffraction-resolution fluorescence imaging. Photochem Photobiol Sci 8(4):465–469
77. Testa I, Wurm CA, Medda R, Rothermel E, von Middendorf C, Folling J, Jakobs S, Schonle A, Hell SW, Eggeling C (2010) Multicolor fluorescence nanoscopy in fixed and living cells by exciting conventional fluorophores with a single wavelength. Biophys J 99(8):2686–2694
78. Lubeck E, Cai L (2012) Single-cell systems biology by super-resolution imaging and combinatorial labeling. Nat Methods 9(7):743–748
79. Hess ST, Gould TJ, Gudheti MV, Maas SA, Mills KD, Zimmerberg J (2007) Dynamic clustered distribution of hemagglutinin resolved at 40 nm in living cell membranes discriminates between raft theories. Proc Natl Acad Sci U S A 104(44):17370–17375
80. Gurskaya NG, Verkhusha VV, Shcheglov AS, Staroverov DB, Chepurnykh TV, Fradkov AF, Lukyanov S, Lukyanov KA (2006) Engineering of a monomeric green-to-red photoactivatable fluorescent protein induced by blue light. Nat Biotechnol 24(4):461–465
81. McKinney SA, Murphy CS, Hazelwood KL, Davidson MW, Looger LL (2009) A bright and photostable photoconvertible fluorescent protein. Nat Methods 6(2):131–133
82. Subach FV, Patterson GH, Renz M, Lippincott-Schwartz J, Verkhusha VV (2010) Bright monomeric photoactivatable red fluorescent protein for two-color super-resolution sptPALM of live cells. J Am Chem Soc 132(18):6481–6491
83. Zhang MS, Chang H, Zhang YD, Yu JW, Wu LJ, Ji W, Chen JJ, Liu B, Lu JZ, Liu YF, Zhang JL, Xu PY, Xu T (2012) Rational design of true monomeric and bright photoactivatable fluorescent proteins. Nat Methods 9(7):727–729
84. Grotjohann T, Testa I, Leutenegger M, Bock H, Urban NT, Lavoie-Cardinal F, Willig KI, Eggeling C, Jakobs S, Hell SW (2011) Diffraction-unlimited all-optical imaging and writing with a photochromic GFP. Nature 478(7368):204–208

85. Brakemann T, Stiel AC, Weber G, Andresen M, Testa I, Grotjohann T, Leutenegger M, Plessmann U, Urlaub H, Eggeling C, Wahl MC, Hell SW, Jakobs S (2011) A reversibly photoswitchable GFP-like protein with fluorescence excitation decoupled from switching. Nat Biotechnol 29(10):942–947
86. Wombacher R, Heidbreder M, van de Linde S, Sheetz MP, Heilemann M, Cornish VW, Sauer M (2010) Live-cell super-resolution imaging with trimethoprim conjugates. Nat Methods 7(9):717–719
87. Lee HL, Lord SJ, Iwanaga S, Zhan K, Xie H, Williams JC, Wang H, Bowman GR, Goley ED, Shapiro L, Twieg RJ, Rao J, Moerner WE (2010) Superresolution imaging of targeted proteins in fixed and living cells using photoactivatable organic fluorophores. J Am Chem Soc 132(43):15099–15101
88. Klein T, Loschberger A, Proppert S, Wolter S, van de Linde SV, Sauer M (2011) Live-cell dSTORM with SNAP-tag fusion proteins. Nat Methods 8(1):7–9
89. Benke A, Manley S (2012) Live-Cell dSTORM of Cellular DNA Based on Direct DNA Labeling. ChemBioChem 13(2):298–301
90. Shim S-H, Xia C, Zhong G, Babcock HP, Vaughan JC, Huang B, Wang X, Xu C, Bi G-Q, Zhuang X (2012) Super-resolution fluorescence imaging of organelles in live cells with photoswitchable membrane probes. Proc Nat Acad Sci U S A 109(35):13978–13983
91. Hell SW (2009) Microscopy and its focal switch. Nat Methods 6(1):24–32
92. Douglass AD, Vale RD (2005) Single-molecule microscopy reveals plasma membrane microdomains created by protein-protein networks that exclude or trap signaling molecules in T cells. Cell 121(6):937–950
93. Manley S, Gillette JM, Patterson GH, Shroff H, Hess HF, Betzig E, Lippincott-Schwartz J (2008) High-density mapping of single-molecule trajectories with photoactivated localization microscopy. Nat Methods 5(2):155–157
94. Giannone G, Hosy E, Levet F, Constals A, Schulze K, Sobolevsky AI, Rosconi MP, Gouaux E, Tampe R, Choquet D, Cognet L (2010) Dynamic superresolution imaging of endogenous proteins on living cells at ultra-high density. Biophys J 99(4):1303–1310
95. Sengupta P, Jovanovic-Talisman T, Skoko D, Renz M, Veatch SL, Lippincott-Schwartz J (2011) Probing protein heterogeneity in the plasma membrane using PALM and pair correlation analysis. Nat Methods 8(11):969–975
96. Subach OM, Patterson GH, Ting L-M, Wang Y, Condeelis JS, Verkhusha VV (2011) A photoswitchable orange-to-far-red fluorescent protein, PSmOrange. Nat Methods 8(9):771–777
97. Goldman RD, Spector DL (2005) Live cell imaging: a laboratory manual. Cold Spring Harbor Laboratory Press. Cold Spring Harbor, New York
98. Fernandez-Suarez M, Ting AY (2008) Fluorescent probes for super-resolution imaging in living cells. Nat Rev Mol Cell Biol 9(12):929–943
99. Dellagiacoma C, Lukinavicius G, Bocchio N, Banala S, Geissbuhler S, Marki I, Johnsson K, Lasser T (2010) Targeted photoswitchable probe for nanoscopy of biological structures. ChemBioChem 11(10):1361–1363
100. Popp MW, Antos JM, Grotenbreg GM, Spooner E, Ploegh HL (2007) Sortagging: a versatile method for protein labeling. Nat Chem Biol 3(11):707–708
101. Fernandez-Suarez M, Baruah H, Martinez-Hernandez L, Xie KT, Baskin JM, Bertozzi CR, Ting AY (2007) Redirecting lipoic acid ligase for cell surface protein labeling with small-molecule probes. Nat Biotechnol 25(12):1483–1487
102. Uttamapinant C, White KA, Baruah H, Thompson S, Fernandez-Suarez M, Puthenveetil S, Ting AY (2010) A fluorophore ligase for site-specific protein labeling inside living cells. Proc Natl Acad Sci U S A 107(24):10914–10919
103. Hoyer P, Staudt T, Engelhardt J, Hell SW (2011) Quantum dot blueing and blinking enables fluorescence nanoscopy. Nano Lett 11(1):245–250
104. Bates M, Blosser TR, Zhuang XW (2005) Short-range spectroscopic ruler based on a single-molecule optical switch. Phys Rev Lett 94(10):108101

105. Conley NR, Biteen JS, Moerner WE (2008) Cy3-Cy5 covalent heterodimers for single-molecule photoswitching. J Phys Chem B 112(38):11878–11880
106. Annibale P, Scarselli M, Kodiyan A, Radenovic A (2010) Photoactivatable fluorescent protein mEos2 displays repeated photoactivation after a long-lived dark state in the red photoconverted form. J Phys Chem Lett 1(9):1506–1510
107. Endesfelder U, Malkusch S, Flottmann B, Mondry J, Liguzinski P, Verveer PJ, Heilemann M (2011) Chemically induced photoswitching of fluorescent probes-a general concept for super-resolution microscopy. Molecules 16(4):3106–3118
108. Annibale P, Vanni S, Scarselli M, Rothlisberger U, Radenovic A (2011) Quantitative photo activated localization microscopy: unraveling the effects of photoblinking. PLoS One 6(7): e22678
109. Lando D, Endesfelder U, Berger H, Subramanian L, Dunne PD, McColl J, Klenerman D, Carr AM, Sauer M, Allshire RC, Heilemann M, Laue ED (2012) Quantitative single-molecule microscopy reveals that CENP-A^{Cnp1} deposition occurs during G2 in fission yeast. Open Biol 2:120078
110. Wiedenmann J, Ivanchenko S, Oswald F, Schmitt F, Rocker C, Salih A, Spindler KD, Nienhaus GU (2004) EosFP, a fluorescent marker protein with UV-inducible green-to-red fluorescence conversion. Proc Natl Acad Sci U S A 101(45):15905–15910
111. Wu M, Huang B, Graham M, Raimondi A, Heuser JE, Zhuang XW, De Camilli P (2010) Coupling between clathrin-dependent endocytic budding and F-BAR-dependent tubulation in a cell-free system. Nat Cell Biol 12(9):902–908
112. Greenfield D, McEvoy AL, Shroff H, Crooks GE, Wingreen NS, Betzig E, Liphardt J (2009) Self-organization of the *Escherichia coli* chemotaxis network imaged with super-resolution light microscopy. PLoS Biol 7(6):e1000137
113. Ptacin JL, Lee SF, Garner EC, Toro E, Eckart M, Comolli LR, Moerner W, Shapiro L (2010) A spindle-like apparatus guides bacterial chromosome segregation. Nat Cell Biol 12(8):791–798
114. Wang WQ, Li GW, Chen CY, Xie XS, Zhuang XW (2011) Chromosome organization by a nucleoid-associated protein in live bacteria. Science 333(6048):1445–1449
115. Lee SF, Thompson MA, Schwartz MA, Shapiro L, Moerner WE (2011) Super-resolution imaging of the nucleoid-associated protein HU in *Caulobacter crescentus*. Biophys J 100(7): L31–33
116. Fu G, Huang T, Buss J, Coltharp C, Hensel Z, Xiao J (2010) In vivo structure of the *E. coli* FtsZ-ring revealed by photoactivated localization microscopy (PALM). PLoS One 5(9): e12682
117. Fleming TC, Shin JY, Lee SH, Becker E, Huang KC, Bustamante C, Pogliano K (2010) Dynamic SpoIIIE assembly mediates septal membrane fission during *Bacillus subtilis* sporulation. Genes Dev 24(11):1160–1172
118. Valtschanoff JG, Weinberg RJ (2001) Laminar organization of the NMDA receptor complex within the postsynaptic density. J Neurosci 21(4):1211–1217
119. Frost NA, Shroff H, Kong HH, Betzig E, Blanpied TA (2010) Single-molecule discrimination of discrete perisynaptic and distributed sites of actin filament assembly within dendritic spines. Neuron 67(1):86–99
120. Watanabe S, Punge A, Hollopeter G, Willig KI, Hobson RJ, Davis MW, Hell SW, Jorgensen EM (2011) Protein localization in electron micrographs using fluorescence nanoscopy. Nat Methods 8(1):80–84
121. Vaughan JC, Jia S, Zhuang XW (2012) Ultrabright photoactivatable fluorophores created by reductive caging. Nat Methods 9(12):1181–1184
122. Izeddin I, El Beheiry M, Andilla J, Ciepielewski D, Darzacq X, Dahan M (2012) PSF shaping using adaptive optics for three-dimensional single-molecule super-resolution imaging and tracking. Opt Express 20(5):4957–4967
123. Baker M (2011) Faster frames, clearer pictures. Nat Methods 8(12):1005–1009

124. Huang ZL, Zhu H, Long F, Ma H, Qin L, Liu Y, Ding J, Zhang Z, Luo Q, Zeng S (2011) Localization-based super-resolution microscopy with an sCMOS camera. Opt Express 19(20):19156–19168
125. Smith CS, Joseph N, Rieger B, Lidke KA (2010) Fast, single-molecule localization that achieves theoretically minimum uncertainty. Nat Methods 7(5):373–375
126. Mortensen KI, Churchman LS, Spudich JA, Flyvbjerg H (2010) Optimized localization analysis for single-molecule tracking and super-resolution microscopy. Nat Methods 7(5):377–381
127. Lippincott-Schwartz J, Patterson GH (2009) Photoactivatable fluorescent proteins for diffraction-limited and super-resolution imaging. Trends Cell Biol 19(11):555–565
128. Vogelsang J, Steinhauer C, Forthmann C, Stein IH, Person-Skegro B, Cordes T, Tinnefeld P (2010) Make them blink: probes for super-resolution microscopy. ChemPhysChem 11(12):2475–2490
129. Dempsey GT, Bates M, Kowtoniuk WE, Liu DR, Tsien RY, Zhuang XW (2009) Photoswitching mechanism of cyanine dyes. J Am Chem Soc 131(51):18192–18193
130. Kottke T, van de Linde S, Sauer M, Kakorin S, Heilemann M (2010) Identification of the product of photoswitching of an oxazine fluorophore using Fourier transform infrared difference spectroscopy. J Phys Chem Lett 1(21):3156–3159
131. van de Linde S, Krstic I, Prisner T, Doose S, Heilemann M, Sauer M (2011) Photoinduced formation of reversible dye radicals and their impact on super-resolution imaging. Photochem Photobiol Sci 10(4):499–506
132. Roeffaers MBJ, De Cremer G, Libeert J, Ameloot R, Dedecker P, Bons AJ, Buckins M, Martens JA, Sels BF, De Vos DE, Hofkens J (2009) Super-resolution reactivity mapping of nanostructured catalyst particles. Angew Chem-Int Edit 48(49):9285–9289
133. Chi KR (2009) Microscopy: Ever-increasing resolution. Nature 462(7273):675–678
134. Baker M (2011) Bright light, better labels. Nature 478(7367):137–142

http://www.springer.com/978-3-662-45546-3

Far-Field Optical Nanoscopy
Tinnefeld, P.; Eggeling, C.; Hell, S.W. (Eds.)
2015, XII, 335 p. 104 illus., 74 illus. in color., Hardcover
ISBN: 978-3-662-45546-3